apM1 (AdiPose Most abundant Gene transcript 1). Biochem Biophys Res Commun 221:286–289.

Martin LJ, Woo JG, Daniels SR, Goodman E, Dolan LM. 2005. The relationships of adiponectin with insulin and lipids are strengthened with increasing adiposity. J Clin Endocrinol Metab 90:4255–4259.

Matsuzawa Y, Funahashi T, Kihara S, Shimomura I. 2004. Adiponectin and metabolic syndrome. Arterioscler Thromb Vasc Biol 24:29–33.

Menzaghi C, Trischitta V, Doria A. 2007. Genetic influences of adiponectin on insulin resistance, type 2 diabetes, and cardiovascular disease. Diabetes 56:1198–1209.

Moldoveanu E, Mut-Vitcu B, Tanaseanu GR, Marta DS, Manea G, Kosaka T, Vidulescu C, Tanaseanu C. 2008. Low basal levels of circulating adiponectin in patients undergoing coronary stenting predict in-stent restenosis, independently of basal levels of inflammatory markers: lipoprotein associated phospholipase A2, and myeloperoxidase. Clin Biochem 41:1429–1433.

Ntalla I, Dedoussis G, Yannakoulia M, Smart MC, Louizou E, Sakka SD, Papoutsakis C, Talmud PJ. 2009. ADIPOQ gene polymorphism rs1501299 interacts with fibre intake to affect adiponectin concentration in children: the GENe-Diet Attica Investigation on childhood obesity. Eur J Nutr 48:493–497.

Pischon T, Girman CJ, Hotamisligil GS, Rifai N, Hu FB, Rimm EB. 2004. Plasma adiponectin levels and risk of myocardial infarction in men. JAMA. 291:1730–1737.

Resink TJ, Kuzmenko YS, Kern F, Stambolsky D, Bochkov VN, Tkachuk VA, Erne P, Niermann T. 1999. LDL binds to surface-expressed human T-cadherin in transfected HEK293 cells and influences homophilic adhesive interactions. FEBS Lett 1463:29–34.

Richards JB, Waterworth D, O'Rahilly S, Hivert MF, Loos RJ, Perry JR, Tanaka T, Timpson NJ, Semple RK, Soranzo N, Song K, Rocha N, Grundberg E, Dupuis J, Florez JC, Langenberg C, Prokopenko I, Saxena R, Sladek R, Aulchenko Y, Evans D, Waeber G, Erdmann J, Burnett MS, Sattar N, Devaney J, Willenborg C, Hingorani A, Witteman JC, Vollenweider P, Glaser B, Hengstenberg C, Ferrucci L, Melzer D, Stark K, Deanfield J, Winogradow J, Grassl M, Hall AS, Egan JM, Thompson JR, Ricketts SL, König IR, Reinhard W, Grundy S, Wichmann HE, Barter P, Mahley R, Kesaniemi YA, Rader DJ, Reilly MP, Epstein SE, Stewart AF, Van Duijn CM, Schunkert H, Burling K, Deloukas P, Pastinen T, Samani NJ, McPherson R, Davey Smith G, Frayling TM, Wareham NJ, Meigs JB, Mooser V, Spector TD; GIANT Consortium. 2009. A genome-wide association study reveals variants in ARL15 that influence adiponectin levels. PLoS Genet 5:e1000768.

Santaniemi M, Kesäniemi YA, Ukkola O. 2006. Low plasma adiponectin concentration is an indicator of the metabolic syndrome. Eur J Endocrinol 155:745–750.

Snehalatha C, Mukesh B, Simon M, Viswanathan V, Haffner SM, Ramachandran A. 2003. Plasma adiponectin is an independent predictor of type 2 diabetes in Asian Indians. Diabetes Care 26:3226–3229.

Wu Y, Li Y, Lange EM, Croteau-Chonka DC, Kuzawa CW, McDade TW, Qin L, Curocichin G, Borja JB, Lange LA, Adair LS, Mohlke KL. 2010. Genome-wide association study for adiponectin levels in Filipino women identifies CDH13 and a novel uncommon haplotype at KNG1-ADIPOQ. Hum Mol Genet 19:4955–4964.

Yamauchi T, Kamon J, Waki H, Terauchi Y, Kubota N, Hara K, Mori Y, Ide T, Murakami K, Tsuboyama-Kasaoka N, Ezaki O, Akanuma Y, Gavrilova O, Vinson C, Reitman ML, Kagechika H, Shudo K, Yoda M, Nakano Y, Tobe K, Nagai R, Kimura S, Tomita M, Froguel P, Kadowaki T. 2001. The fat-derived hormone adiponectin reverses insulin resistance associated with both lipoatrophy and obesity. Nat Med 7:941–946.

Yang WS, Chuang LM. 2006. Human genetics of adiponectin in the metabolic syndrome. J Mol Me 84:112–121.

Yu YH, Ginsberg HN. 2005. Adipocyte signaling and lipid homeostasis: sequelae of insulin-resistant adipose tissue. Circ Res 96:1042–1052.

Electrophysiological Consequences of Dyssynchronous Heart Failure and Its Restoration by Resynchronization Therapy

Takeshi Aiba, MD, PhD; Geoffrey G. Hesketh, BS; Andreas S. Barth, MD; Ting Liu, PhD; Samantapudi Daya, MD; Khalid Chakir, PhD; Veronica Lea Dimaano, MD; Theodore P. Abraham, MD; Brian O'Rourke, PhD; Fadi G. Akar, PhD; David A. Kass, MD; Gordon F. Tomaselli, MD

Background—Cardiac resynchronization therapy (CRT) is widely applied in patients with heart failure and dyssynchronous contraction (DHF), but the electrophysiological consequences of CRT in heart failure remain largely unexplored.

Methods and Results—Adult dogs underwent left bundle-branch ablation and either right atrial pacing (190 to 200 bpm) for 6 weeks (DHF) or 3 weeks of right atrial pacing followed by 3 weeks of resynchronization by biventricular pacing at the same pacing rate (CRT). Isolated left ventricular anterior and lateral myocytes from nonfailing (control), DHF, and CRT dogs were studied with the whole-cell patch clamp. Quantitative polymerase chain reaction and Western blots were performed to measure steady state mRNA and protein levels. DHF significantly reduced the inward rectifier K^+ current (I_{K1}), delayed rectifier K^+ current (I_K), and transient outward K^+ current (I_{to}) in both anterior and lateral cells. CRT partially restored the DHF-induced reduction of I_{K1} and I_K but not I_{to}, consistent with trends in the changes in steady state K^+ channel mRNA and protein levels. DHF reduced the peak inward Ca^{2+} current (I_{Ca}) density and slowed I_{Ca} decay in lateral compared with anterior cells, whereas CRT restored peak I_{Ca} amplitude but did not hasten decay in lateral cells. Calcium transient amplitudes were depressed and the decay was slowed in DHF, especially in lateral myocytes. CRT hastened the decay in both regions and increased the calcium transient amplitude in lateral but not anterior cells. No difference was found in $Ca_V1.2$ (α1C) mRNA or protein expression, but reduced $Ca_V\beta2$ mRNA was found in DHF cells. DHF reduced phospholamban, ryanodine receptor, and sarcoplasmic reticulum Ca^{2+} ATPase and increased Na^+-Ca^{2+} exchanger mRNA and protein. CRT did not restore the DHF-induced molecular remodeling, except for sarcoplasmic reticulum Ca^{2+} ATPase. Action potential durations were significantly prolonged in DHF, especially in lateral cells, and CRT abbreviated action potential duration in lateral but not anterior cells. Early afterdepolarizations were more frequent in DHF than in control cells and were reduced with CRT.

Conclusions—CRT partially restores DHF-induced ion channel remodeling and abnormal Ca^{2+} homeostasis and attenuates the regional heterogeneity of action potential duration. The electrophysiological changes induced by CRT may suppress ventricular arrhythmias, contribute to the survival benefit of this therapy, and improve the mechanical performance of the heart. (***Circulation.*** **2009;119:1220-1230.)**

Key Words: ion channels ■ remodeling ■ heart failure ■ resynchronization ■ electrophysiology

Nearly 5 million Americans have heart failure (HF), and >250 000 die annually. Up to 50% of deaths in patients with HF are sudden and unexpected, mainly because of lethal ventricular arrhythmias such as ventricular tachycardia and ventricular fibrillation[1]; however, the mechanisms of ventricular tachycardia and ventricular fibrillation in patients with HF remain controversial.[1,2]

Editorial p 1192
Clinical Perspective p 1230

As HF progresses, the heart adapts to intrinsic and extrinsic stresses through a complex process of chamber remodeling and molecular modifications of myocyte structure and function. The structural remodeling and alteration of cell-to-cell coupling are associated with heterogeneous conduction delays in the ventricular myocardium that can lead to dyssynchronous ventricular contraction.[3] Dyssynchronous contraction adversely influences the electrical phenotype of the failing heart and has been associated with regional changes in calcium (Ca^{2+}) handling protein expression[4] and exaggerated heterogeneities in conduction[5] and repolarization,[6–8] which enhances the susceptibility to ventricular arrhythmias in HF.[9] Predictably, advanced HF with dyssynchronous cardiac contraction (DHF) is associated with a poor prognosis.[10] Cardiac

Received May 28, 2008; accepted November 7, 2008.
From the Division of Cardiology, Johns Hopkins University School of Medicine, Baltimore, Md.
The online-only Data Supplement is available with this article at http://circ.ahajournals.org/cgi/content/full/CIRCULATIONAHA.108.794834/DC1.
Correspondence to Gordon F. Tomaselli, MD, Michel Mirowski, MD, Professor of Cardiology, Chief of Cardiology, Johns Hopkins University, Baltimore, MD 21205. E-mail gtomasel@jhmi.edu

Circulation **is available at http://circ.ahajournals.org** **DOI: 10.1161/CIRCULATIONAHA.108.794834**

resynchronization therapy (CRT) with biventricular pacing improves symptoms,[11] cardiac function, and mortality,[12,13] presumably due to a reduction in stress-strain disparities and improvement in the efficiency of ventricular contraction. We have recently demonstrated that CRT reverses regional molecular remodeling and reduces apoptosis.[14]

Ion channel remodeling in HF underlies many of the changes in cellular electrophysiology and predisposes to atrial and ventricular arrhythmias in animal models and patients with HF.[1,2,15–20] A consistent electrophysiological consequence of HF is a prolongation of ventricular repolarization, which is due in part to functional downregulation of outward potassium currents.[2,15–17,19–21] However, little information is available about regional differences in ion channel function and expression or action potential (AP) profiles between early- and late-activated regions of dyssynchronous contracting left ventricles (LVs). Furthermore, the extent to which CRT reverses the DHF-induced electrophysiological remodeling remains unexplored.

Here, we tested the hypothesis that dyssynchronous mechanical contraction in HF contributes significantly to pathological remodeling at the cellular and molecular levels. We studied whether and to what extent remodeling could be reversed by biventricular pacing. We characterized the regional differences of AP, ionic currents, and $[Ca^{2+}]_i$ transients (CaT) in myocytes isolated from the anterior and lateral LV myocardium of dogs with DHF and CRT and correlated the cellular electrophysiological changes with their subunit mRNA and protein expression in corresponding regions of the LV. These findings suggest distinct mechanisms of altered electrophysiological remodeling in DHF, as well as reverse remodeling by CRT. These data provide new mechanistic understanding of the therapeutic role of CRT and will help to identify new antiarrhythmic targets to prevent sudden death in patients with HF.

Methods

An expanded Methods section is available in the online-only Data Supplement.

Canine Tachypacing-Induced HF Model

All protocols followed US Department of Agriculture and National Institutes of Health guidelines and were approved by the Animal Care and Use Committee of the Johns Hopkins Medical Institutions. The canine models of DHF or CRT have been described previously.[5,14,22] In brief, adult male mongrel dogs underwent left bundle-branch radiofrequency ablation and right atrial pacing (190 to 200 bpm) for 6 weeks (DHF dogs; n=7) or 3 weeks of right atrial pacing followed by 3 weeks of resynchronization by biventricular pacing at the same pacing rate (CRT dogs; n=7).

ECG, Echocardiography, and Hemodynamic Recordings

To monitor LV function during tachypacing, 2-dimensional echocardiography with tissue Doppler imaging was performed periodically together with recordings of ECGs. Briefly, standard 2-dimensional and color Doppler image data, triggered to the QRS complex, were saved in cine-loop format. LV volumes (end-systolic and end-diastolic) and LV ejection fraction were calculated from the conventional apical 2- and 4-chamber views. LV dyssynchrony was quantified with speckle-tracking radial strain analysis (Figure 1) as described previously.[23] The LV dyssynchrony index was defined as the SD of time to peak systolic velocity of 12 segments. Standard 12-lead ECG and hemodynamic data (LV systolic and end-diastolic pressure, dP/dt_{max}) were recorded 6 weeks after the start of pacing.

Patch Clamp and CaT

All electrophysiological and intracellular Ca^{2+} measurements were performed at physiological temperature (37°C). All methods for cell isolation, electrophysiological recording, and measurements are routine in our laboratory and have been described previously.[4,8,16,17,20] Isolated ventricular myocytes from the anterior and lateral mid myocardium were current and voltage clamped by the standard whole-cell patch-clamp technique for measurement of APs, transient outward K^+ current (I_{to}), inward rectifier K^+ current (I_{K1}), delayed rectifier K^+ currents (I_K), and Ca^{2+} current (I_{Ca}). Borosilicate glass electrodes with tip resistances of ≈3.0 MΩ when filled with the pipette solution were used.

CaTs were measured by indo-1 fluorescence excited at 365 nm with a xenon arc lamp, and emitted light at 405 and 495 nm was collected with a 2-channel photomultiplier tube assembly. Fluorescence signals were digitized and stored with electrophysiological recordings for offline analysis with custom software.[24] The ratio of indo-1 fluorescence ($R=F_{405\ nm}/F_{495\ nm}$) was determined after subtraction of cellular autofluorescence. The rate of Ca^{2+} removal (τ_{Ca}) was determined by fitting a single exponential to the Ca^{2+} time course.

Molecular Analysis

Canine Kir2.1, $K_V4.3$, KChIP2, $K_V11.1$ (ether a-go-go related gene [ERG]), Kv7.1 (KvLQT1), minK, $Ca_V1.2$ (α1C), $Ca_V\beta1$, $Ca_V\beta2$, sarcoplasmic reticulum Ca^{2+}ATPase (SERCA2), phospholamban, ryanodine receptor, and Na^+-Ca^{2+} exchanger steady state mRNA levels were measured by reverse-transcription polymerase chain reaction in tissue isolated from the LV anterior and lateral walls in control, DHF, and CRT dogs (online-only Data Supplement Table I). Kir2.1, $K_V4.3$, KChIP2, ERG, KvLQT1, $Ca_V1.2$ (α1C), SERCA2, phospholamban, ryanodine receptor, and Na^+-Ca^{2+} exchanger proteins were measured by Western immunoblotting. Detailed methods are provided in the online-only Data Supplement.

Statistical Analysis

Differences among multiple groups were compared by ANOVA with Bonferroni test. Two-group analysis was performed by t test (paired or unpaired as appropriate). Differences in serial studies were assessed by repeated-measures ANOVA. Data are expressed as mean±SD or mean±SEM as indicated in each of the Figures. A value of $P<0.05$ was considered significant.

The authors had full access to and take full responsibility for the integrity of the data. All authors have read and agree to the manuscript as written.

Results

ECG and Hemodynamic Changes

Figure 1 shows representative standard ECG and LV wall strain plots by tissue Doppler from a control (A), 6-week paced DHF (B), and CRT (C) dog. In the DHF dog, the QRS interval was wider, with a left bundle-branch block pattern compared with the control, and the tissue Doppler image showed dyssynchronous contraction between the septum and the lateral walls. CRT shortened the QRS duration and resynchronized the LV wall strain pattern so that it was similar to the control.

The Table summarizes the ECG, echocardiographic, and hemodynamic changes in control, 6-week paced DHF, and CRT dogs. In sinus rhythm, the R-R interval was shorter and the corrected QT and QRS durations were longer in both DHF and CRT dogs than in control dogs, but no significant difference was observed in these parameters between DHF and CRT dogs. However, during pacing, QRS width was significantly shorter in CRT than DHF dogs, which was

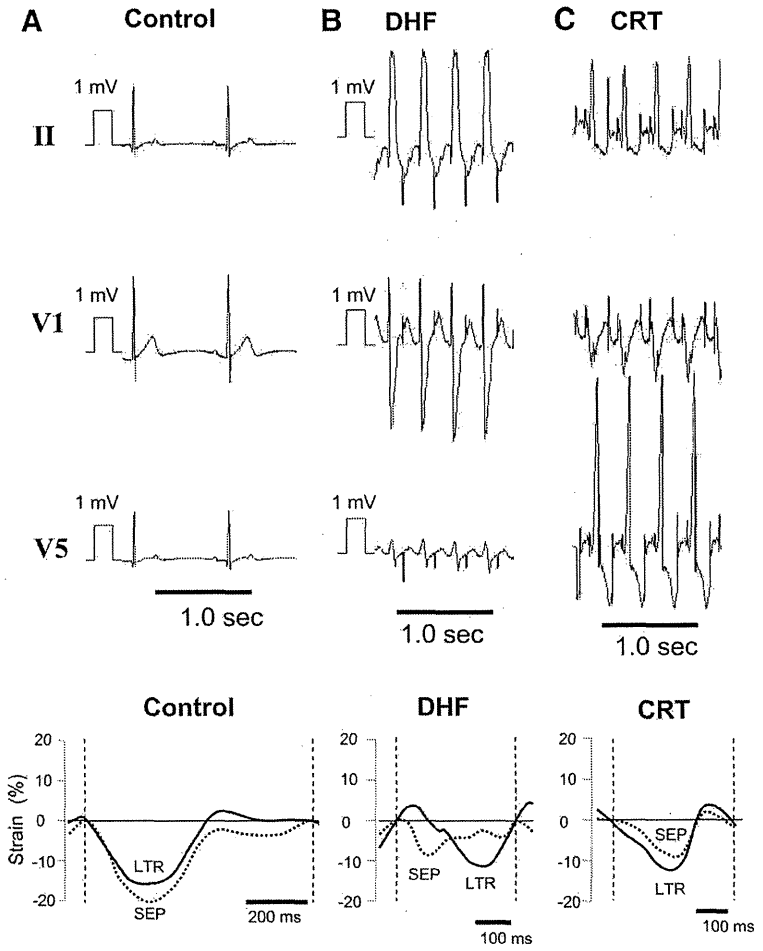

Figure 1. Representative ECGs and changes of LV septal (SEP) and lateral (LTR) strain from control (A), 6-week paced DHF (B), and CRT (C) dogs. ECGs from DHF and CRT dogs are shown during pacing, and control is shown during sinus rhythm. Biventricular pacing synchronized the strain patterns between LV septal and lateral walls and abbreviated the DHF-induced prolongation of QRS duration.

consistent with the larger dyssynchrony index by tissue Doppler echocardiography in DHF compared with control or CRT dogs. Moreover, CRT significantly decreased the corrected QT interval compared with DHF. Conversely, LV diastolic and systolic volumes, as well as hemodynamic parameters such as LV end-diastolic and end-systolic pressure and dP/dt_{max}, were not statistically different between DHF and CRT. A trend was observed toward increased stroke volume and ejection fraction in CRT versus DHF dogs.

Cell Capacitance

Cell capacitance was larger in DHF and CRT than in control dogs in cells isolated from both the anterior and lateral walls, but no regional difference was found between anterior and lateral cells. The capacitance of cells isolated from CRT dogs was not different from that of cells isolated from DHF dogs (online-only Data Supplement Table II).

Inward Rectifier K^+ Current

Figure 2A shows whole-cell I_{K1} currents in lateral myocytes from control, DHF, and CRT dogs. The densities of I_{K1} from control and DHF myocytes were similar to data previously reported from our laboratory.[16] I_{K1} density in DHF myocytes was reduced significantly compared with control, whereas CRT partially reversed the DHF-induced reduction of I_{K1} over a wide voltage range (Figure 2B). On the other hand, no regional difference was found in I_{K1} between anterior and lateral myocytes isolated from either DHF or CRT hearts (Figure 2C). The relevant component of I_{K1} for AP repolarization is the outward current "hump" observed at potentials positive to the K^+ reversal potential. The peak outward component of I_{K1} at -70 and -60 mV was decreased modestly but significantly ($P<0.05$) in DHF myocytes (1.43 ± 0.52 and 1.07 ± 0.43 pA/pF, respectively) compared with control (1.78 ± 0.54 and 1.26 ± 0.51 pA/pF, respectively) and CRT (1.81 ± 0.81 and 1.18 ± 0.57 pA/pF, respectively). To investigate the molecular basis for changes in I_{K1}, we measured Kir2.1 mRNA and protein levels; these were significantly downregulated in DHF compared with control ($P<0.05$), whereas those in CRT were decreased (although not statistically significant) compared with control (Figures 2D and 2E). No regional differences in Kir2.1 mRNA and protein expression were found among the 3 groups, which is consistent with the cellular electrophysiology.

Transient Outward K^+ Current

Figure 3A shows whole-cell I_{to} currents in lateral myocytes from control, DHF, and CRT dogs. The densities of I_{to} from control and DHF myocytes in this preparation are similar to those reported previously in our laboratory.[16] I_{to} in DHF myocytes was reduced significantly compared with control ($P<0.05$), but CRT did not restore the DHF-induced reduction of I_{to} (Figure 3B). Interestingly, I_{to} current density was not different between

Table. ECG, Echocardiography, and Hemodynamic Parameters

	Control	DHF	CRT
ECG, ms			
Sinus rhythm			
RR	608±115	438±34*	428±34*
QT	278±31	286±43	300±15*
QTc	359±26	434±64*	467±38*
QRS	47±6	103±21*	102±10*
Pacing			
RR	...	314±14	308±18
QT	...	280±23	239±39
QTc	...	489±35	429±58†
QRS	...	112±16	64±6†
Echocardiography			
DI, ms	30±5	74±25*	29±23†
LVEDV, mL	52±6	87±18*	93±20*
LVESV, mL	17±4	64±17*	63±15*
SV, %	35±6	23±12*	29±15
LVEF, %	67±7	25±12*	30±11*
Hemodynamics			
HR, bpm	105±26	151±42*	150±12*
LVEDP, mm Hg	6±5	35±8*	34±10*
LVESP, mm Hg	142±27	103±19*	101±10*
dP/dt_{max} mm Hg/s	1900±467	831±246*	846±133*

QTc indicates corrected QT; DI, dyssynchrony index; LVEDV, LV end-diastolic volume; LVESV, LV end-systolic volume; SV, stroke volume; LVEF, LV ejection fraction; HR, heart rate; LVEDP, LV end-diastolic pressure; and LVESP, LV end-systolic pressure.

Values are mean±SD.

*$P<0.05$ vs control; †$P<0.05$ vs DHF.

anterior and lateral myocytes in any group (Figure 3C). To investigate the molecular basis for change in I_{to}, we measured the α-subunit (Kv4.3) and β-subunit (KChIP2) underlying this current (Figures 3D through 3G). Consistent with the I_{to} density, both Kv4.3 and KChIP2 mRNA and protein were significantly downregulated in both DHF and CRT, with no regional differences in each group.

Delayed Rectifier K^+ Currents

Figure 4A shows total I_K in lateral myocytes from control, DHF, and CRT dogs. As shown in the superimposed currents elicited by a step pulse to +50 mV, the peak and tail I_K currents were smaller in DHF than in control myocytes, and CRT partially restored the DHF-induced reduction of I_K. Figure 4B displays the current-voltage relationship of the tail current density of I_K in the 3 groups, showing that DHF reduced I_K density by ≈50% compared with control, whereas CRT partially restored the DHF-induced reduction of I_K ($P<0.05$). In addition, no regional difference was found in the reduction and restoration of I_K by DHF and CRT (Figure 4C).

To investigate the molecular basis for changes in I_K, we measured the expression of the underlying α-subunit ($K_V7.1$ [K_VLQT1] for I_{Ks} and $K_V11.1$ [ERG] for I_{Kr}) and β-subunit (minK for I_{Ks}) mRNA and proteins. KvLQT1 mRNA and

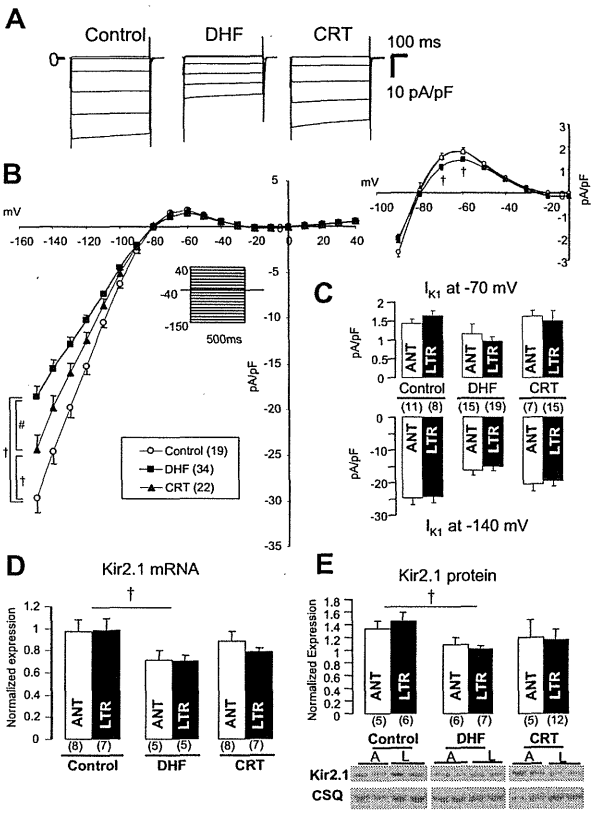

Figure 2. I_{K1} and Kir2.1 mRNA and protein levels in control, DHF, and CRT. A, Representative current traces in lateral myocytes isolated from control, DHF, and CRT canine ventricles elicited by the diagrammed voltage-clamp protocol (holding potential −40 mV, test pulse 500 ms in duration). B, Steady state current-voltage (I-V) relationship of I_{K1} and outward current portion of the I-V (right) in each group. The voltage-clamp protocol is shown in the inset. C, I_{K1} density at −140 and −70 mV in anterior (ANT) and lateral (LTR) myocytes of each group. D and E, Kir2.1 mRNA and protein expression in anterior and lateral myocytes of each group. A or ANT indicates anterior; L or LTR, lateral; and CSQ, calsequestrin. †$P<0.05$ vs control; #$P<0.05$ vs DHF. The values in parentheses are the number of cells or tissue samples studied in this and all remaining figures.

protein were reduced significantly in DHF compared with control myocytes; CRT did not alter KvLQT1 mRNA expression but increased the protein level such that it was not significantly different from control (Figure 4D and 4E). No significant differences were found in minK mRNA expression among the 3 groups (Figure 4F). ERG mRNA expression was reduced in DHF and completely restored by CRT (Figure 4G), but no significant difference was found in ERG protein expression in any of the groups (Figure 4H). In addition, consistent with the physiological data, no regional differences in gene or protein expression were found between anterior and lateral LV tissues from each group.

Inward Ca^{2+} Current (I_{Ca}) and CaT

Figure 5A shows I_{Ca} in LV midmyocardial myocytes isolated from control, DHF, and CRT hearts. In control, no difference was found in the peak I_{Ca} density or current decay between anterior and lateral myocytes; however, DHF reduced the peak I_{Ca} density and slowed the rate of current decay in lateral

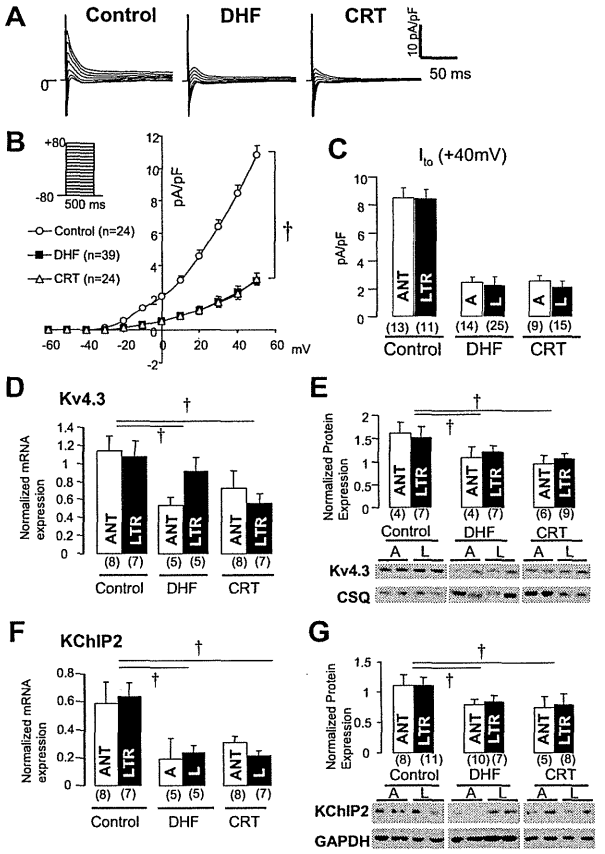

Figure 3. I_{to}, and its underlying subunit mRNA and protein expression in control, DHF, and CRT. A, Representative current traces in lateral myocytes from control, DHF, and CRT ventricles elicited by the voltage-clamp protocol shown in inset. B, Peak current-voltage relationship of I_{to} in each group. C, I_{to} density at +40 mV in anterior and lateral myocytes of each group. D through G, Kv4.3 and KChIP2 mRNA and protein expression in LV midmyocardial tissue isolated from control, DHF, and CRT dogs. A or ANT indicates anterior; L or LTR, lateral; and CSQ, calsequestrin. †$P<0.05$ vs control.

cells compared with anterior cells. Furthermore, in CRT, no regional difference was found in peak I_{Ca} density, but the rate of current decay was still slower in lateral than in anterior cells. The current-voltage relationships (Figure 5B) showed that peak I_{Ca} density was significantly less in lateral cells than in anterior cells in DHF at voltage steps from −15 to +20 mV ($P<0.05$). In contrast, CRT increased I_{Ca} density in lateral cells but not in anterior cells.

Although the voltage dependence of activation of I_{Ca} (Figure 5C) was not altered significantly in either DHF or CRT compared with control in either anterior or lateral cells, the rate of current decay (Figure 5D) in DHF was significantly slower (41.7±9.5 versus 33.9±5.4 ms, $P<0.05$) in lateral cells and significantly faster (25.6±4.0 versus 32.1±5.3 ms, $P<0.05$) in anterior cells than in control cells, and this produced a robust difference in current decay between anterior and lateral cells in DHF. Moreover, CRT slowed the DHF-induced faster current decay in anterior cells (32.8±7.4 ms, $P<0.05$) but did not affect the rate of I_{Ca} decay in lateral cells (40.4±9.3 ms). Therefore, the total charge carried by I_{Ca} (Figure 5E) was not altered significantly by DHF in either anterior or lateral cells. On the other hand, CRT significantly increased the charge carried by I_{Ca} in lateral (from 0.14±0.04 to 0.19±0.06 pC/pF, $P<0.05$) but not anterior cells compared with control.

CaTs (Figure 5F) were not different in anterior and lateral cells from control hearts; however, DHF significantly reduced the CaT amplitude and slowed the rate of decay of the CaT most prominently in lateral myocytes. CRT hastened the DHF-induced slowing of the decay of the CaT without changing the amplitude in anterior cells, whereas CaT amplitude was increased and decay hastened significantly in lateral cells. The changes in amplitude and rate of decay of CaT in each group are shown in Figure 5G and 5H, respectively. Notably, CRT almost fully reversed the DHF-induced smaller amplitude and longer decay of CaT.

Molecular Basis for Abnormal Ca^{2+} Homeostasis

The molecular basis for changes in I_{Ca} and CaT was investigated by determining the steady state levels of $Ca_V1.2$ ($Ca_V\alpha1C$), $Ca_V\beta1$, $Ca_V\beta2$, ryanodine receptor, phospholamban, SERCA2, and Na^+-Ca^{2+} exchanger mRNA and protein (Figure 6). No significant differences in $Ca_V1.2$ mRNA and protein or $Ca_V\beta1$ subunit mRNA expression were found among control, DHF, and CRT hearts (Figure 6A through 6C). On the other hand, $Ca_V\beta2$ mRNA was decreased significantly in DHF but not CRT myocytes compared with control (Figure 6D). Steady state ryanodine receptor and phospholamban mRNA and protein expression were consistently lower in both DHF and CRT myocytes than in control (Figure 6E through 6H), and SERCA2 mRNA and protein levels were reduced significantly in DHF myocytes but were not decreased significantly in CRT (Figure 6I and 6J). On the other hand, Na^+-Ca^{2+} exchanger mRNA expression (Figure 6K) was increased significantly in CRT ($P<0.05$) compared with control, and protein levels were increased in both DHF and CRT (Figure 6L). However, no regional difference was found in the steady state levels of Ca^{2+} channel or homeostasis-related genes and proteins in each group.

APs and Early Afterdepolarizations

Figure 7A shows superimposed APs elicited at pacing cycle lengths of 0.5, 1.0, 2.0, and 4.0 seconds in anterior and lateral myocytes from control, DHF, and CRT dogs. Compared with control, DHF prolonged the action potential duration (APD) at all pacing cycle lengths, more prominently in lateral than in anterior cells. In contrast, CRT partially reversed the DHF-induced prolongation of APD in lateral cells but not in anterior cells. The relationship between APD and pacing cycle length of each group (Figure 7B) revealed that APD in both DHF and CRT cells was similarly prolonged in anterior cells, and the slope of the APD–cycle length relationship was increased, whereas in lateral cells, a prominent prolongation of APD in DHF was found, particularly at long pacing cycle lengths, which resulted in a significant difference in APD between anterior and lateral cells ($P<0.05$). By selectively shortening the APD of lateral myocytes, CRT reduced the regional heterogeneity in APD compared with DHF. The resting membrane potential (Figure 7C) was not signifi-

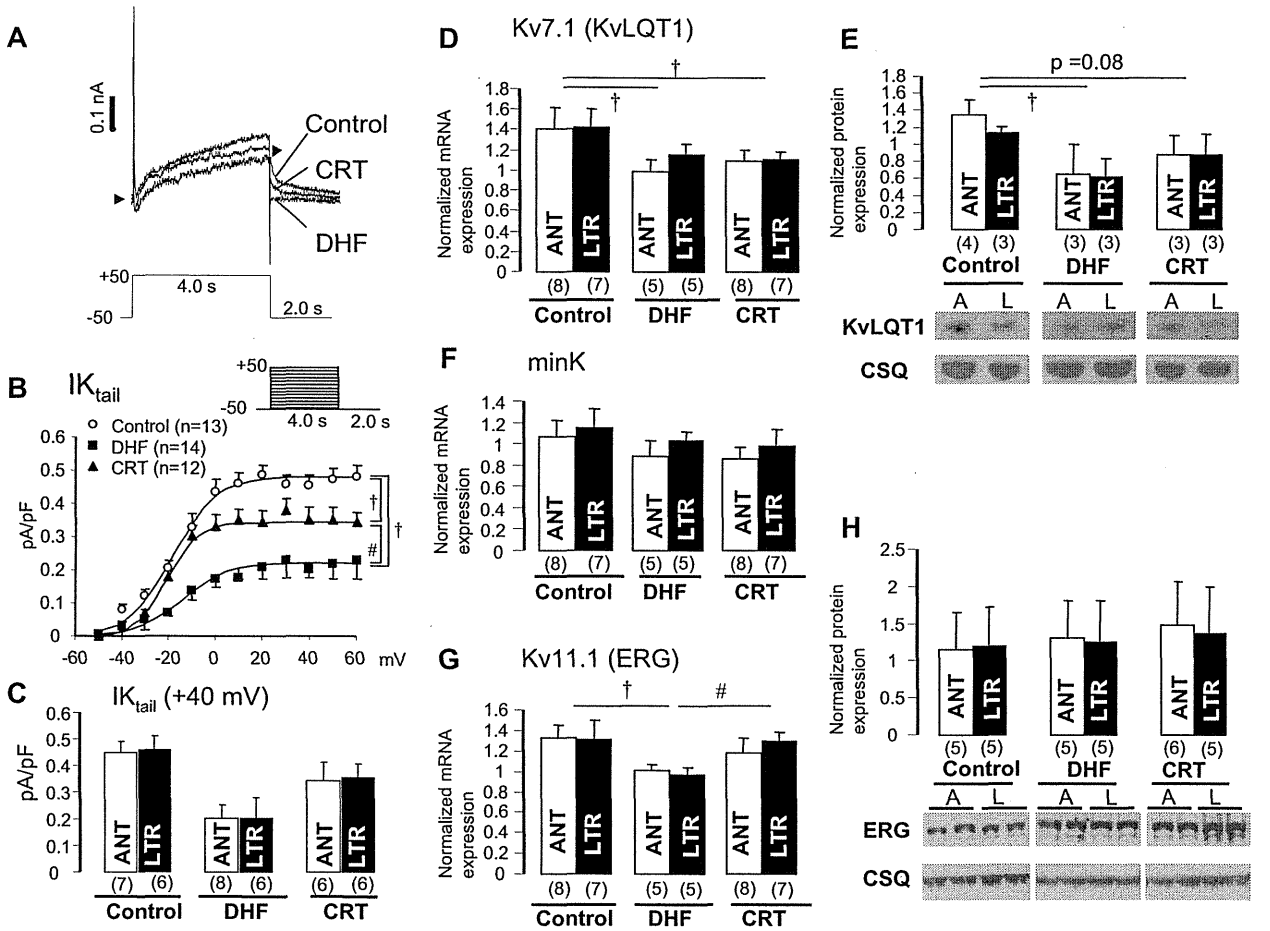

Figure 4. I_K and its underlying subunit mRNA and protein expression in control, DHF, and CRT hearts. A, Representative current traces from control, DHF, and CRT myocytes elicited by voltage-clamp protocol shown in the inset. B, Current-voltage relationship of the tail current of I_K ($I_{K\ tail}$) fitted to the Boltzmann equation: $I_{K,tail}=1/\{1+\exp[(V_{1/2}-V_m)/k]\}$. Voltage-clamp protocol is shown in the inset. C, $I_{K\ tail}$ density at 40 mV between anterior and lateral myocytes in each group. D through H, KvLQT1, minK, and ERG mRNA and protein expression in mid myocardium of control, DHF, and CRT dogs. A or ANT indicates anterior; L or LTR, lateral; and CSQ, calsequestrin. †$P<0.05$ vs control; #$P<0.05$ vs DHF.

cantly different between control, DHF, and CRT dogs, whereas the phase 1 notch depth (Figure 7D) was significantly attenuated in DHF and CRT dogs, consistent with no restoration of I_{to} by CRT.

Early afterdepolarizations (EADs) were observed more frequently in DHF than in control myocytes ($P<0.001$), and CRT significantly reduced the frequency of EADs compared with DHF ($P<0.05$; Figure 8A); however, no regional differences were found in development of EADs between anterior and lateral cells in each group. Figure 8B shows representative APs with [EAD(+)] or without [EAD(−)] EADs in myocytes from DHF hearts. The APD at 90% recovery (APD_{90}) was modestly but significantly longer in EAD(+) myocytes than in EAD(−) myocytes; however, the APD at 20% recovery (APD_{20}) was markedly shorter in EAD(+) myocytes than in EAD(−) myocytes. Therefore, we examined the relationship between the APD_{20}, APD_{90}, and APD_{20}/APD_{90} ratio and EAD development in the failing myocytes (Figure 8C; online-only Data Supplement Table III). APD_{20} was shorter and APD_{90} longer in EAD(+) cells than in EAD(−) cells, which resulted in a dramatically smaller APD_{20}/APD_{90} ratio in EAD(+) myocytes.

Discussion

Our studies reveal the regional cellular electrophysiological consequences of synchronous and dyssynchronous ventricular contraction in the failing heart and include several novel insights into electrophysiological remodeling in HF. First, CRT partially reverses DHF-induced K^+ channel remodeling (I_{K1} and I_K) in both the anterior and lateral LV. An interesting divergence in the remodeling of K^+ currents can be seen: CRT has no effect on DHF-induced downregulation of I_{to} or on the expression of Kv4.3 or KChIP2 mRNA or protein. Second, Ca^{2+} current remodeling and Ca^{2+} handling were significantly different in the anterior and lateral LV in DHF, and CRT significantly improved Ca^{2+} homeostasis, especially in the lateral wall. Third, the APD was significantly prolonged in DHF, especially in cells isolated from the lateral LV, and CRT abbreviated the APD in lateral cells and reduced the regional gradient of APD. Finally, EADs were more frequent in DHF, were significantly but not completely reduced to near control levels in CRT, and were associated with a modestly prolonged APD_{90} and a markedly reduced APD_{20}/APD_{90} ratio. It is important to recognize that the model that we used corrects dyssynchronous contraction but does not affect

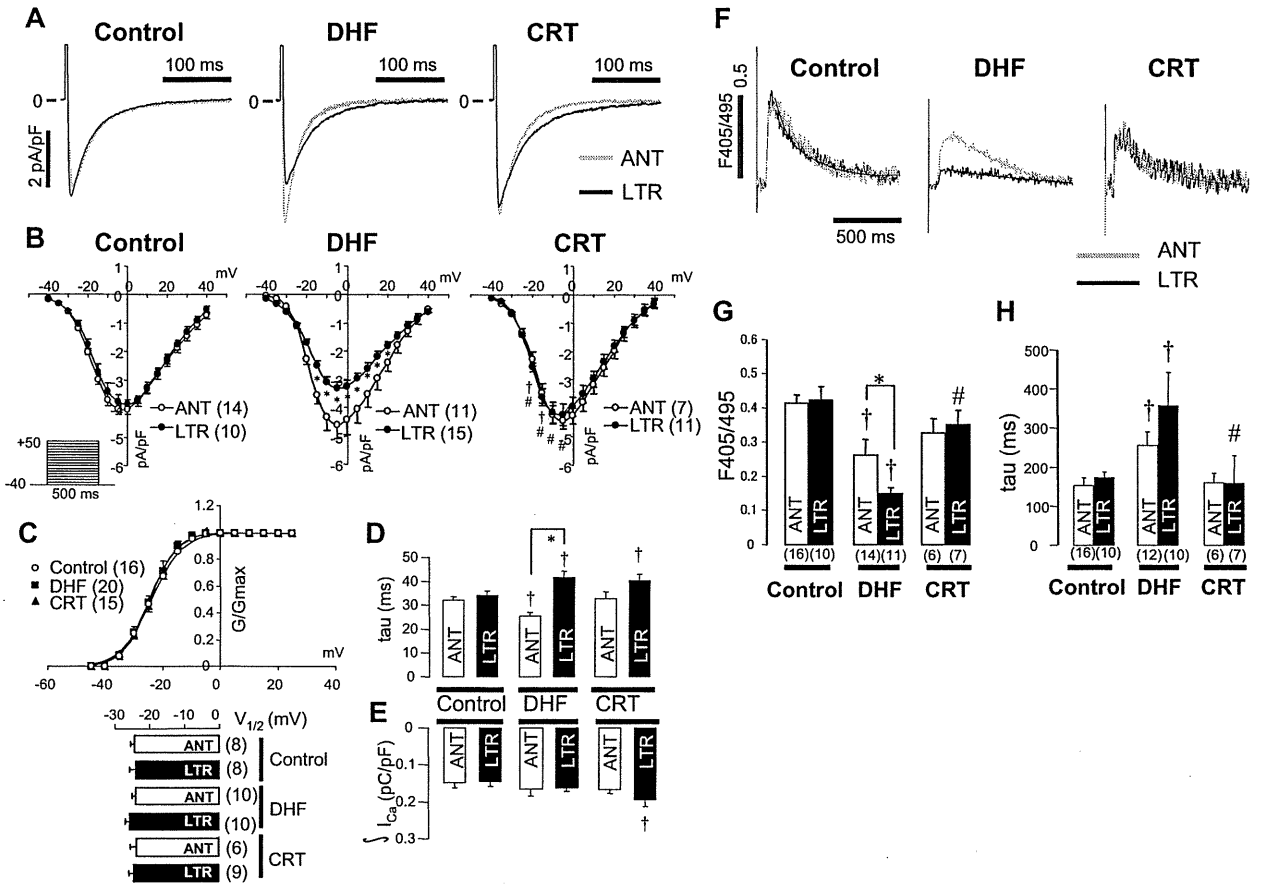

Figure 5. I_{Ca} and CaT in control, DHF, and CRT dogs. A, Representative I_{Ca} recorded from anterior and lateral myocytes. B, Peak current-voltage relationships for $I_{Ca,L}$ in control, DHF, and CRT myocytes. Voltage-clamp protocol is shown in the inset. C, Voltage dependence of I_{Ca} activation in control, DHF, and CRT myocytes was fit with a Boltzmann equation of the form $G/G_{max}=1/[1+\exp(V_{1/2}-V)/k]$. The voltage at which G_{Ca} was half-maximal ($V_{1/2}$) did not differ among the 3 groups and regions. D, Plot of the time constant of the fast (major) component of current decay measured at 0 mV. E, Plot of the charge carried by I_{Ca} during the first 200 ms of the voltage step. F, Representative superimposed CaTs recorded in anterior and lateral myocytes from control, DHF, and CRT dogs stimulated at 0.5 Hz as measured with indo-1 fluorescence. G and H, Average peak fluorescence values and average decay τ of CaT measured at 0.5-Hz stimulation frequency in anterior and lateral myocytes from control, DHF, and CRT dogs. ANT indicates anterior; LTR, lateral. †$P<0.05$ vs control; #$P<0.05$ vs DHF by ANOVA; *$P<0.05$ by t test, anterior vs lateral.

tachycardia-induced LV dysfunction. Thus, the reversal of DHF-induced electrical and Ca^{2+} handling remodeling by CRT is due to the effect of electrical resynchronization by biventricular pacing.

K^+ Channel Remodeling

Downregulation of K^+ currents is the most consistent ionic current change in animal models[1,16,20,21] and human HF.[15] K^+ current downregulation may promote ventricular tachycardia and ventricular fibrillation,[21] either by direct prolongation of AP[19] in the voltage range at which $I_{Ca,L}$ reactivation occurs, which predisposes to the development of EADs,[25] or by heterogeneous reduction of the repolarization reserve and the promotion of functional reentry. Although expressed cardiac K^+ channels vary in different species, I_{to} downregulation is the most consistent ionic current change in failing mammalian hearts.[15,16,20,21] In the present study, I_{to} and its related genes, Kv4.3 and KChIP2, were downregulated homogenously by DHF and were not affected by CRT. The data suggest that tachycardia, HF, or altered ventricular activation is more important in downregulation of I_{to} than mechanical synchrony. Reduced I_{K1} density in HF[16,18,20] may contribute to prolongation of APD and enhanced susceptibility to spontaneous membrane depolarization.[26] Although small but significant changes in I_{K1} density were observed in the outward current component, and the largest changes were observed at very negative voltages (Figure 2B and 2C), the resting membrane potential of myocytes did not differ in any of the groups (Figure 7C), because the major voltage range of altered I_{K1} was beyond physiological potentials. On the other hand, in tachypacing-induced HF models, I_{Ks} is downregulated, but I_{Kr} is less consistent.[18,21] In the present study, both I_{K1} and I_K densities were reduced in a regionally homogenous fashion by DHF in spite of the higher wall stress and myocyte stretch in the late-activated lateral wall than in the early-activated anterior wall[27]; this was partially but significantly restored by CRT without a change in global LV function, which suggests that K^+ channel remodeling was not directly associated with the mechanical stress caused by dyssynchronous ventricular contraction.

The dichotomy in the regulation of I_{to} compared with I_{K1} and I_K in CRT is remarkable. These currents share regulatory

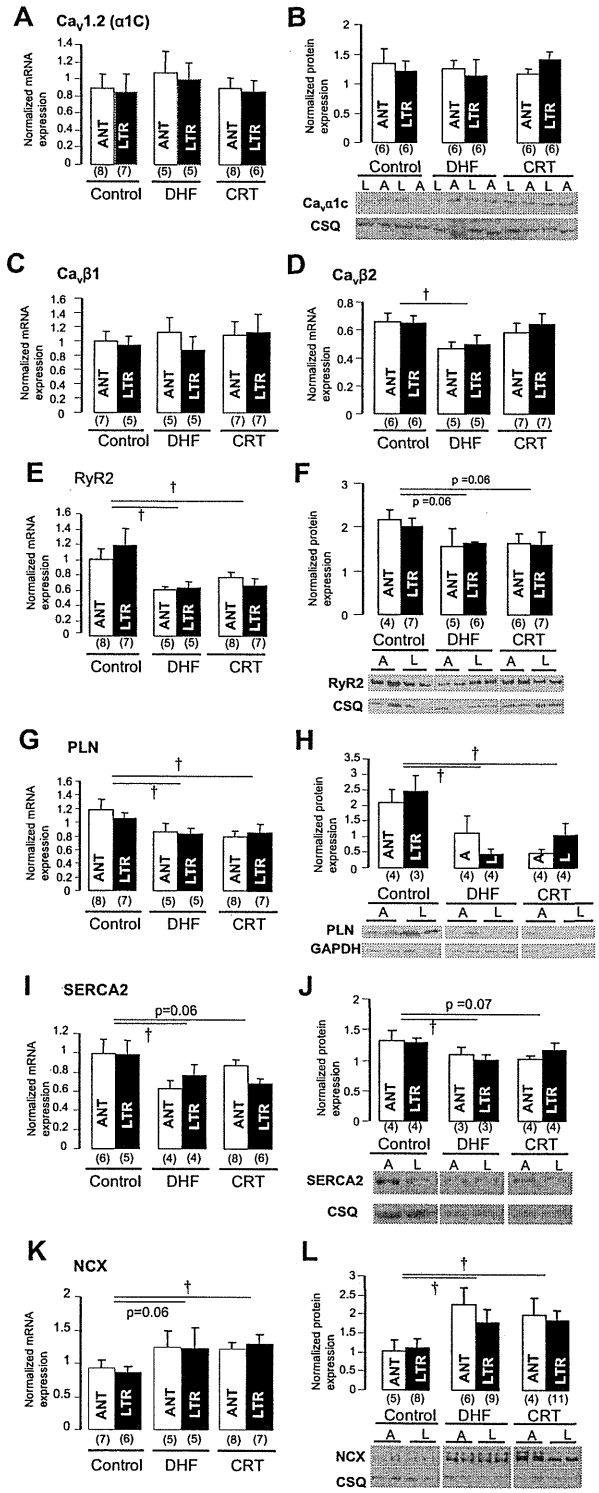

Figure 6. Ca^{2+} handling–related mRNA and protein expression in control, DHF, and CRT myocytes. A and B, Cav1.2 (α1c) mRNA and protein. C and D, Ca_Vβ1 and Ca_Vβ2 mRNA. E and F, Ryanodine receptor (RyR2) mRNA and protein. G and H, Phospholamban (PLN) mRNA and protein. I and J, SERCA2 mRNA and protein. K and L, Na^+-Ca^{2+} exchanger (NCX) mRNA and protein. A or ANT indicates anterior; L or LTR, lateral; and CSQ, calsequestrin. †P<0.05 vs control.

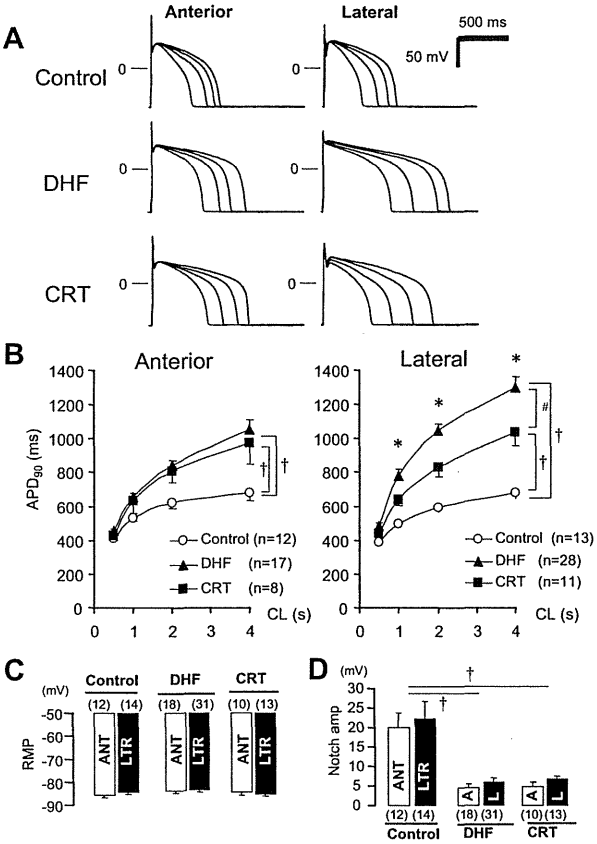

Figure 7. APD in LV myocytes from control, DHF, and CRT hearts. A, Representative superimposed APs recorded at pacing cycle lengths (CL) of 0.5, 1.0, 2.0, and 4.0 seconds, B, Relationship between pacing CL and APD at 90% recovery (APD_{90}) from anterior and lateral myocytes in each group. C and D, Bar plot of resting membrane potential (RMP; C) and phase 1 notch amplitude (D) at pacing CL of 2.0 seconds. †P<0.05 vs control; #P<0.05 vs DHF; *P<0.05 vs anterior. ANT or A indicates anterior; LTR or L, lateral.

mechanisms that are altered in the failing heart and are differentially remodeled by CRT.[14] The detailed regulation by the autonomic nervous system, renin-angiotensin-aldosterone signaling, and reactive oxygen species are distinct for each of the K^+ currents studied and may explain the differences in response to CRT. In addition, biventricular tachypacing in the present study improved the synchrony of mechanical contraction, but global LV function as assessed by LV ejection fraction or end-diastolic pressure was still significantly depressed. It is likely that the molecular mechanisms for the altered functional expression of each current are mixed. The steady state levels of Kv4.3 and KChIP2 mRNA are consistently downregulated by tachypacing in the presence and absence of mechanical synchrony; thus, the balance between transcription and RNA degradation is altered. Furthermore, altered ventricular activation by CRT may suppress I_{to} expression independent of the presence of HF.[28,29] Concordant changes in protein levels suggest the possibility of a pretranslational mechanism. However, the reduction in Kv4.3 and KChIP2 proteins in particular is not as pronounced as the magnitude of the current reduction, which suggests an additional posttranslational mechanism of functional downregu-

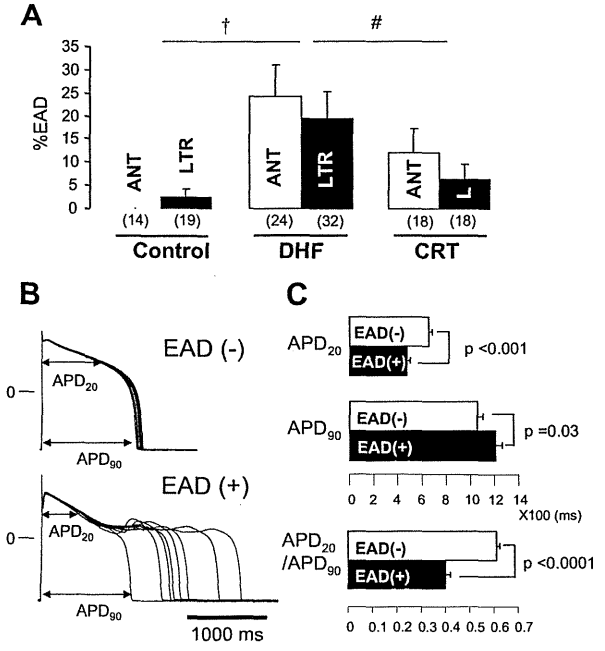

Figure 8. EADs in myocytes from control, DHF, and CRT hearts. A, Bar plot of frequency of EADs (%EADs indicates fraction of APs with EADs). B, Representative superimposed APs recorded in myocytes isolated from lateral wall of DHF hearts with [EAD(+)] or without [EAD(−)] EADs. C, Bar plots of APD_{20}, APD_{90}, and ratio of APD_{20} to APD_{90} (APD_{20}/APD_{90}) in failing myocytes. All data were obtained during pacing at 0.25 Hz. †$P<0.05$ vs control; #$P<0.05$ vs DHF. ANT or A indicates anterior; LTR or L, lateral.

lation of I_{to}. The changes in I_{K1} and Kir2.1 mRNA and protein in DHF and CRT appear to be more consistent with but not proof of a pretranslational mechanism of downregulation. Changes in KvLQT1 and ERG mRNA and protein are more variable and appear to be partially altered by CRT. There appear to be distinct differences in the mechanism of downregulation of individual K^+ currents in DHF and variable degrees and mechanisms of restoration of expression in CRT.

Altered I_{Ca} and Ca^{2+} Handling

Changes in I_{Ca} functional expression in HF are variable.[30] Depending on the model and stage of HF, some studies showed a decrease in I_{Ca} density, whereas others reported no change.[2,16,31] In the present study, the peak I_{Ca} density and current decay in DHF were regionally different between myocytes isolated from the lower-stress anterior and higher-stress lateral walls. Furthermore, CRT regionally restored the DHF-induced changes in I_{Ca}, increasing the peak I_{Ca} density in lateral cells and slowing the decay in anterior cells; CRT thus served to mitigate the DHF-induced regional heterogeneities in I_{Ca} density and gating.

HF causes significant changes in Ca^{2+}-handling proteins.[2,32] In failing human hearts, the steady state level of the $Ca_V1.2(\alpha 1C)$ mRNA was reported to be decreased[33] or unchanged.[17] Moreover, Vanderheyden et al[34] recently suggested the possibility of reverse molecular remodeling of SERCA2 in CRT responders. In the present study, $Ca_V1.2(\alpha 1C)$ mRNA and protein were not different between control, DHF, and CRT dogs, consistent with our previous data in human myocardium.[17]

Ca_V β-subunit expression has been positively correlated with peak $Ca_V1.2$ current density.[35] The present data showed that $Ca_V\beta 1$ mRNA levels were unchanged in DHF and CRT, whereas steady state $Ca_V\beta 2$ mRNA levels were reduced in DHF and partially restored by CRT. In DHF, ryanodine receptor, phospholamban, and SERCA2a mRNA and protein levels were downregulated, whereas Na^+-Ca^{2+} exchanger was upregulated, consistent with previous studies.[4,31,36,37] No regional differences in mRNA and protein expression were found in any of these mediators of Ca^{2+} handling in DHF and CRT, which suggests that the regional differences of Ca^{2+} handling in DHF and its restoration by CRT are posttranslational.

The mechanisms underlying the differences in regional remodeling of K^+ currents and Ca^{2+} handling in DHF remain obscure. Plotnikov et al[7] reported that cardiac dyssynchrony by LV pacing (120 to 150 bpm for 3 weeks) produced a slower decay of I_{Ca} inactivation, consistent with the present results. Moreover, this phenomenon was suppressed by β-adrenergic blockade. These findings suggest that DHF-induced changes of I_{Ca} inactivation kinetics might be mediated by regionally heterogeneous β-adrenergic receptor stimulation. Furthermore, the Ca^{2+}-handling proteins are functionally regulated by phosphorylation, prominently by the key intracellular enzymes protein kinase A and Ca^{2+}-calmodulin–dependent protein kinase II (CaMKII),[38–40] as well as a variety of phosphatases that may be regionally regulated.[14]

Prolongation of APD and Development of EADs

The APD is consistently prolonged in human and animal models of HF.[2,15–17,19–21] A recent study using a canine model of dyssynchrony suggests that after 4 weeks, the APD is prolonged in the late-activated compared with the early-activated regions.[6] In the present work, CRT produced a partial but statistically significant shortening of DHF-induced prolongation of APD selectively in lateral cells. Although the peak I_{Ca} density in DHF was decreased in lateral cells compared with anterior cells, the decrease was modest and not significant compared with control lateral myocytes (Figure 5B). On the other hand, I_{Ca} decay was slowed significantly, which might contribute to regional AP prolongation in the setting of homogenous K^+ current downregulation, although Ca^{2+} flux through L-type channels during a square pulse protocol does not fully reflect that during an AP. These data provide some insight into the mechanism of regional AP remodeling in DHF and CRT.

Moreover, on a molecular level, we have shown that tumor necrosis factor-α and CaMKII were increased in DHF, prominently in the lateral wall, and these differences were absent in CRT.[14] Tumor necrosis factor-α decreases I_{to} and prolongs APD in rat ventricular myocytes.[41] CaMKII influences Ca^{2+} current and sarcoplasmic reticulum function[39,40] and increases persistent Na^+ current,[42,43] which results in prolongation of APD.[44] It is possible, and indeed likely, that other regional alterations in Ca^{2+} handling (Figure 5F) or an increased persistent Na^+ current contribute to regional differences in the APD and AP profile in DHF and to the regionally specific effects of biventricular pacing on this phenotype. Furthermore, EADs were observed more frequently in DHF

than in control myocytes, and CRT reduced the occurrence of EADs in both anterior and lateral cells.

Prolongation of APD_{90} was associated with an increased frequency of EADs, but notably, a smaller APD_{20}/APD_{90} ratio was even more strongly correlated with the appearance of EADs (Figure 8C). Thus, APD prolongation alone may not be sufficient to generate EADs in failing myocytes.[44] The APD_{20}/APD_{90} ratio is an empiric metric but suggests that long APs with a reduced plateau voltage are the most likely to exhibit EADs. This type of AP profile that is generated by the reduction in K^+ current density and reduced I_{Ca} density with slowed kinetics is highly susceptible to EADs that result from reactivation of I_{Ca}.

Study Limitations

The model of DHF and CRT used in the present study is a limitation. Six weeks of tachypacing (200 bpm) reproducibly induces dilated cardiomyopathy with LV enlargement, increased LV end-diastolic pressure, and decreased dP/dt_{max}; however, the study was designed to examine the effects of CRT with ongoing HF, and thus, tachypacing was maintained. This differs from CRT in patients, which is performed at lower heart rates. Therefore, the processes of both remodeling and the reversal of remodeling in this circumstance are likely to be different from those in human DHF.

The second limitation is that the present study focused on the cellular and molecular bases of electrophysiological remodeling in DHF and restoration by CRT. It did not evaluate the susceptibility to and frequent development of arrhythmia in vivo or in a whole-heart model.

Clinical Implications

CRT has emerged as an effective pacing/mechanical therapy for patients with HF and a prolonged QRS duration. CRT has been associated with improved cardiac function, symptomatology, and exercise capacity and, when combined with defibrillator therapy, reduced mortality.[12,13] The role of CRT in preventing arrhythmias[45,46] or reversing adverse electrical remodeling remains controversial. The present study provides novel information on the altered expression and function of ionic currents and CaTs in DHF and after CRT. Understanding the fundamental mechanisms of the altered ion channel function and Ca^{2+} homeostasis, as well as the electrophysiological remodeling in DHF, and the capacity for restoration by CRT will not only help define the therapeutic role of CRT but will help to identify antiarrhythmic targets that can be exploited by other therapeutic strategies designed to prevent sudden death.

Acknowledgments

The authors thank Yanli Tian, Deborah DiSilvestre, Victoria Halperin, and Richard S. Tunin for excellent technical support.

Sources of Funding

The work was supported by National Institutes of Health grants P01 HL 077180 (to Drs Kass and Tomaselli) and HL 072488 (to Dr Tomaselli) and a grant from Medtronic Japan (to Dr Aiba). Dr Tomaselli is the Michel Mirowski, MD, Professor in Cardiology.

Disclosures

Dr Tomaselli has received a research grant from Boston Scientific. The remaining authors report no conflicts.

References

1. Tomaselli GF, Zipes DP. What causes sudden death in heart failure? *Circ Res.* 2004;95:754–763.
2. Nattel S, Maguy A, Le Bouter S, Yeh YH. Arrhythmogenic ion-channel remodeling in the heart: heart failure, myocardial infarction, and atrial fibrillation. *Physiol Rev.* 2007;87:425–456.
3. Grines CL, Bashore TM, Boudoulas H, Olson S, Shafer P, Wooley CF. Functional abnormalities in isolated left bundle branch block: the effect of interventricular asynchrony. *Circulation.* 1989;79:845–853.
4. Spragg DD, Leclercq C, Loghmani M, Faris OP, Tunin RS, DiSilvestre D, McVeigh ER, Tomaselli GF, Kass DA. Regional alterations in protein expression in the dyssynchronous failing heart. *Circulation.* 2003;108:929–932.
5. Spragg DD, Akar FG, Helm RH, Tunin RS, Tomaselli GF, Kass DA. Abnormal conduction and repolarization in late-activated myocardium of dyssynchronously contracting hearts. *Cardiovasc Res.* 2005;67:77–86.
6. Jeyaraj D, Wilson LD, Zhong J, Flask C, Saffitz JE, Deschenes I, Yu X, Rosenbaum DS. Mechanoelectrical feedback as novel mechanism of cardiac electrical remodeling. *Circulation.* 2007;115:3145–3155.
7. Plotnikov AN, Yu H, Geller JC, Gainullin RZ, Chandra P, Patberg KW, Friezema S, Danilo P Jr, Cohen IS, Feinmark SJ, Rosen MR. Role of L-type calcium channels in pacing-induced short-term and long-term cardiac memory in canine heart. *Circulation.* 2003;107:2844–2849.
8. Pak PH, Nuss HB, Tunin RS, Kaab S, Tomaselli GF, Marban E, Kass DA. Repolarization abnormalities, arrhythmia and sudden death in canine tachycardia-induced cardiomyopathy. *J Am Coll Cardiol.* 1997;30:576–584.
9. Akar FG, Spragg DD, Tunin RS, Kass DA, Tomaselli GF. Mechanisms underlying conduction slowing and arrhythmogenesis in nonischemic dilated cardiomyopathy. *Circ Res.* 2004;95:717–725.
10. Bader H, Garrigue S, Lafitte S, Reuter S, Jais P, Haissaguerre M, Bonnet J, Clementy J, Roudaut R. Intra-left ventricular electromechanical asynchrony: a new independent predictor of severe cardiac events in heart failure patients. *J Am Coll Cardiol.* 2004;43:248–256.
11. Abraham WT, Fisher WG, Smith AL, Delurgio DB, Leon AR, Loh E, Kocovic DZ, Packer M, Clavell AL, Hayes DL, Ellestad M, Trupp RJ, Underwood J, Pickering F, Truex C, McAtee P, Messenger J. Cardiac resynchronization in chronic heart failure. *N Engl J Med.* 2002;346:1845–1853.
12. Cleland JG, Daubert JC, Erdmann E, Freemantle N, Gras D, Kappenberger L, Tavazzi L. The effect of cardiac resynchronization on morbidity and mortality in heart failure. *N Engl J Med.* 2005;352:1539–1549.
13. Bristow MR, Saxon LA, Boehmer J, Krueger S, Kass DA, De Marco T, Carson P, DiCarlo L, DeMets D, White BG, DeVries DW, Feldman AM. Cardiac-resynchronization therapy with or without an implantable defibrillator in advanced chronic heart failure. *N Engl J Med.* 2004;350:2140–2150.
14. Chakir K, Daya SK, Tunin RS, Helm RH, Byrne MJ, Dimaano VL, Lardo AC, Abraham TP, Tomaselli GF, Kass DA. Reversal of global apoptosis and regional stress kinase activation by cardiac resynchronization. *Circulation.* 2008;117:1369–1377.
15. Beuckelmann DJ, Nabauer M, Erdmann E. Alterations of K+ currents in isolated human ventricular myocytes from patients with terminal heart failure. *Circ Res.* 1993;73:379–385.
16. Kaab S, Nuss HB, Chiamvimonvat N, O'Rourke B, Pak PH, Kass DA, Marban E, Tomaselli GF. Ionic mechanism of action potential prolongation in ventricular myocytes from dogs with pacing-induced heart failure. *Circ Res.* 1996;78:262–273.
17. Kaab S, Dixon J, Duc J, Ashen D, Nabauer M, Beuckelmann DJ, Steinbeck G, McKinnon D, Tomaselli GF. Molecular basis of transient outward potassium current downregulation in human heart failure: a decrease in Kv4.3 mRNA correlates with a reduction in current density. *Circulation.* 1998;98:1383–1393.
18. Li GR, Lau CP, Ducharme A, Tardif JC, Nattel S. Transmural action potential and ionic current remodeling in ventricles of failing canine hearts. *Am J Physiol Heart Circ Physiol.* 2002;283:H1031–H1041.
19. Akar FG, Rosenbaum DS. Transmural electrophysiological heterogeneities underlying arrhythmogenesis in heart failure. *Circ Res.* 2003;93:638–645.
20. Rose J, Armoundas AA, Tian Y, DiSilvestre D, Burysek M, Halperin V, O'Rourke B, Kass DA, Marban E, Tomaselli GF. Molecular correlates of

altered expression of potassium currents in failing rabbit myocardium. *Am J Physiol Heart Circ Physiol.* 2005;288:H2077–H2087.
21. Tsuji Y, Zicha S, Qi XY, Kodama I, Nattel S. Potassium channel subunit remodeling in rabbits exposed to long-term bradycardia or tachycardia: discrete arrhythmogenic consequences related to differential delayed-rectifier changes. *Circulation.* 2006;113:345–355.
22. Leclercq C, Faris O, Tunin R, Johnson J, Kato R, Evans F, Spinelli J, Halperin H, McVeigh E, Kass DA. Systolic improvement and mechanical resynchronization does not require electrical synchrony in the dilated failing heart with left bundle-branch block. *Circulation.* 2002;106:1760–1763.
23. Abraham TP, Dimaano VL, Liang HY. Role of tissue Doppler and strain echocardiography in current clinical practice. *Circulation.* 2007;116: 2597–2609.
24. O'Rourke B, Kass DA, Tomaselli GF, Kaab S, Tunin R, Marban E. Mechanisms of altered excitation-contraction coupling in canine tachycardia-induced heart failure, I: experimental studies. *Circ Res.* 1999; 84:562–570.
25. Aiba T, Shimizu W, Inagaki M, Noda T, Miyoshi S, Ding WG, Zankov DP, Toyoda F, Matsuura H, Horie M, Sunagawa K. Cellular and ionic mechanism for drug-induced long QT syndrome and effectiveness of verapamil. *J Am Coll Cardiol.* 2005;45:300–307.
26. Nuss HB, Kaab S, Kass DA, Tomaselli GF, Marban E. Cellular basis of ventricular arrhythmias and abnormal automaticity in heart failure. *Am J Physiol.* 1999;277:H80–H91.
27. Helm RH, Byrne M, Helm PA, Daya SK, Osman NF, Tunin R, Halperin HR, Berger RD, Kass DA, Lardo AC. Three-dimensional mapping of optimal left ventricular pacing site for cardiac resynchronization. *Circulation.* 2007;115:953–961.
28. Yu H, McKinnon D, Dixon JE, Gao J, Wymore R, Cohen IS, Danilo P Jr, Shvilkin A, Anyukhovsky EP, Sosunov EA, Hara M, Rosen MR. Transient outward current, I_{to1}, is altered in cardiac memory. *Circulation.* 1999;99:1898–905.
29. Patberg KW, Plotnikov AN, Quamina A, Gainullin RZ, Rybin A, Danilo P Jr, Sun LS, Rosen MR. Cardiac memory is associated with decreased levels of the transcriptional factor CREB modulated by angiotensin II and calcium. *Circ Res.* 2003;93:472–478.
30. Pitt GS, Dun W, Boyden PA. Remodeled cardiac calcium channels. *J Mol Cell Cardiol.* 2006;41:373–388.
31. Armoundas AA, Rose J, Aggarwal R, Stuyvers BD, O'Rourke B, Kass DA, Marban E, Shorofsky SR, Tomaselli GF, William Balke C. Cellular and molecular determinants of altered Ca2+ handling in the failing rabbit heart: primary defects in SR Ca2+ uptake and release mechanisms. *Am J Physiol Heart Circ Physiol.* 2007;292:H1607–H1618.
32. Bers DM. Cardiac excitation-contraction coupling. *Nature.* 2002;415: 198–205.
33. Takahashi T, Allen PD, Lacro RV, Marks AR, Dennis AR, Schoen FJ, Grossman W, Marsh JD, Izumo S. Expression of dihydropyridine receptor (Ca2+ channel) and calsequestrin genes in the myocardium of patients with end-stage heart failure. *J Clin Invest.* 1992;90:927–935.
34. Vanderheyden M, Mullens W, Delrue L, Goethals M, de Bruyne B, Wijns W, Geelen P, Verstreken S, Wellens F, Bartunek J. Myocardial gene expression in heart failure patients treated with cardiac resynchronization therapy: responders versus nonresponders. *J Am Coll Cardiol.* 2008;51: 129–136.
35. Miriyala J, Nguyen T, Yue DT, Colecraft HM. Role of CaVβ subunits, and lack of functional reserve, in protein kinase A modulation of cardiac CaV1.2 channels. *Circ Res.* 2008;102:e54–e64.
36. Pogwizd SM, Qi M, Yuan W, Samarel AM, Bers DM. Upregulation of Na^+/Ca^{2+} exchanger expression and function in an arrhythmogenic rabbit model of heart failure. *Circ Res.* 1999;85:1009–1019.
37. Hobai IA, O'Rourke B. Enhanced Ca^{2+}-activated Na^+-Ca^{2+} exchange activity in canine pacing-induced heart failure. *Circ Res.* 2000;87: 690–698.
38. Ai X, Curran JW, Shannon TR, Bers DM, Pogwizd SM. Ca^{2+}/calmodulin-dependent protein kinase modulates cardiac ryanodine receptor phosphorylation and sarcoplasmic reticulum Ca^{2+} leak in heart failure. *Circ Res.* 2005;97:1314–1322.
39. Kohlhaas M, Zhang T, Seidler T, Zibrova D, Dybkova N, Steen A, Wagner S, Chen L, Brown JH, Bers DM, Maier LS. Increased sarcoplasmic reticulum calcium leak but unaltered contractility by acute CaMKII overexpression in isolated rabbit cardiac myocytes. *Circ Res.* 2006;98:235–244.
40. Maier LS, Zhang T, Chen L, DeSantiago J, Brown JH, Bers DM. Transgenic CaMKIIδC overexpression uniquely alters cardiac myocyte Ca^{2+} handling: reduced SR Ca^{2+} load and activated SR Ca^{2+} release. *Circ Res.* 2003;92:904–911.
41. Fernandez-Velasco M, Ruiz-Hurtado G, Hurtado O, Moro MA, Delgado C. TNF-alpha downregulates transient outward potassium current in rat ventricular myocytes through iNOS overexpression and oxidant species generation. *Am J Physiol Heart Circ Physiol.* 2007;293:H238–H245.
42. Wagner S, Dybkova N, Rasenack EC, Jacobshagen C, Fabritz L, Kirchhof P, Maier SK, Zhang T, Hasenfuss G, Brown JH, Bers DM, Maier LS. Ca^{2+}/calmodulin-dependent protein kinase II regulates cardiac Na^+ channels. *J Clin Invest.* 2006;116:3127–3138.
43. Maltsev VA, Reznikov V, Undrovinas NA, Sabbah HN, Undrovinas A. Modulation of late sodium current by Ca2+, calmodulin, and CaMKII in normal and failing dog cardiomyocytes: similarities and differences. *Am J Physiol Heart Circ Physiol.* 2008;294:H1597–H1608.
44. Wu Y, Temple J, Zhang R, Dzhura I, Zhang W, Trimble R, Roden DM, Passier R, Olson EN, Colbran RJ, Anderson ME. Calmodulin kinase II and arrhythmias in a mouse model of cardiac hypertrophy. *Circulation.* 2002;106:1288–1293.
45. Medina-Ravell VA, Lankipalli RS, Yan GX, Antzelevitch C, Medina-Malpica NA, Medina-Malpica OA, Droogan C, Kowey PR. Effect of epicardial or biventricular pacing to prolong QT interval and increase transmural dispersion of repolarization: does resynchronization therapy pose a risk for patients predisposed to long QT or torsade de pointes? *Circulation.* 2003;107:740–746.
46. Fish JM, Di Diego JM, Nesterenko V, Antzelevitch C. Epicardial activation of left ventricular wall prolongs QT interval and transmural dispersion of repolarization: implications for biventricular pacing. *Circulation.* 2004;109:2136–2142.

CLINICAL PERSPECTIVE

Cardiac resynchronization therapy (CRT) with biventricular pacing improves symptoms, cardiac function, and exercise capacity, and when combined with defibrillator therapy, it reduces mortality in patients with heart failure who have dyssynchronous contraction (DHF). CRT reduces stress-strain disparities and thus improves the efficiency of contraction of the ventricle. However, the role of CRT in preventing arrhythmias or reversing adverse electrical remodeling remains controversial. The present study provides novel information on the altered regional expression and function of ionic currents and calcium (Ca^{2+}) transients in DHF and partial restoration by CRT in a canine pacing-induced DHF model. CRT partially restores the DHF-induced reduction of selected K^+ currents and significantly improves Ca^{2+} homeostasis, especially in the lateral wall of the left ventricle. The overall effect of CRT is abbreviation of the DHF-induced prolongation of action potential duration in cells isolated from the lateral left ventricle, thus reducing the regional action potential duration gradient and the frequency of potentially arrhythmogenic early afterdepolarizations compared with DHF. Thus, CRT partially reverses both the cellular triggers and substrate for arrhythmias in DHF.

Pathological Role of Serum- and Glucocorticoid-Regulated Kinase 1 in Adverse Ventricular Remodeling

Saumya Das, MD, PhD; Takeshi Aiba, MD, PhD; Michael Rosenberg, MD; Katherine Hessler, BA; Chunyang Xiao, PhD; Pablo A. Quintero, MD; Filomena G. Ottaviano, PhD; Ashley C. Knight, BSc; Evan L. Graham, MSc; Pontus Boström, MD, PhD; Michael R. Morissette, PhD; Federica del Monte, MD, PhD; Michael J. Begley, PhD; Lewis C. Cantley, PhD; Patrick T. Ellinor, MD, PhD; Gordon F. Tomaselli, MD; Anthony Rosenzweig, MD

Background—Heart failure is a growing cause of morbidity and mortality. Cardiac phosphatidylinositol 3-kinase signaling promotes cardiomyocyte survival and function, but it is paradoxically activated in heart failure, suggesting that chronic activation of this pathway may become maladaptive. Here, we investigated the downstream phosphatidylinositol 3-kinase effector, serum- and glucocorticoid-regulated kinase-1 (SGK1), in heart failure and its complications.

Methods and Results—We found that cardiac SGK1 is activated in human and murine heart failure. We investigated the role of SGK1 in the heart by using cardiac-specific expression of constitutively active or dominant-negative SGK1. Cardiac-specific activation of SGK1 in mice increased mortality, cardiac dysfunction, and ventricular arrhythmias. The proarrhythmic effects of SGK1 were linked to biochemical and functional changes in the cardiac sodium channel and could be reversed by treatment with ranolazine, a blocker of the late sodium current. Conversely, cardiac-specific inhibition of SGK1 protected mice after hemodynamic stress from fibrosis, heart failure, and sodium channel alterations.

Conclusions—SGK1 appears both necessary and sufficient for key features of adverse ventricular remodeling and may provide a novel therapeutic target in cardiac disease. **(*Circulation*. 2012;126:2208-2219.)**

Key Words: arrhythmia ■ heart failure ■ ion channels or ion channel ■ signal transduction

Cardiovascular disease remains the dominant cause of morbidity and mortality in industrialized nations. Heart failure is associated with altered electric properties of cardiomyocytes[1,2] including prolongation of action potential duration (APD). These changes, in combination with cardiac structural changes, are termed electric remodeling and comprise the triggers and substrates of ventricular arrhythmia, an important cause of sudden cardiac death. Electric remodeling frequently occurs in association with adverse mechanical remodeling and cardiac dysfunction. In heart failure, an increase in persistent sodium current (late I_{Na} or I_{NaL})[1] can contribute to APD prolongation, although the pathways leading to I_{NaL} are incompletely understood. Thus, our understanding of electric and mechanical remodeling in heart disease remains incomplete.

Editorial see p 2175
Clinical Perspective on p 2219

Acute activation of phosphatidylinositol 3-kinase signaling promotes cardiomyocyte survival and function.[3–5] Surprisingly, proximal phosphatidylinositol 3-kinase signaling is enhanced in patients with cardiac dysfunction and heart failure,[6,7] raising the possibility that initially compensatory activation of this pathway becomes maladaptive and contributes to adverse remodeling. In this context, serum- and glucocorticoid-regulated kinase-1 (SGK1) is a particularly intriguing candidate. SGK1 is a phosphatidylinositol 3-kinase–dependent, serine-threonine kinase that is structurally similar to Akt.[8] SGK1 expression is transcriptionally regulated by mineralocorticoid signaling,[9] an important contributor to heart failure and arrhythmia. SGK1 regulates sodium ion transport in the kidney[10] and in heterologous expression systems,[11] and thus could mechanistically link phosphatidylinositol 3-kinase signaling, heart failure, and arrhythmia.

We previously found that cardiac SGK1 is activated early after pressure overload induced by transverse aortic constriction (TAC) and that acute activation promotes cardiomyocyte survival.[5] Here we demonstrate that SGK1 is also persistently activated in TAC-induced heart failure (TAC-HF) in mice,

Received April 30, 2012; accepted August 17, 2012.

From the Cardiovascular Institute (S.D., M.R., K.H., C.X., P.A.Q., F.G.O., A.C.K., E.G.L., M.R.M., F.D., A.R.), Division of Signal Transduction Unit and Cancer Center (M.J.B., L.C.C.), Beth Israel Deaconess Medical Center, Boston, MA; Division of Cardiology, Johns Hopkins University School of Medicine, Baltimore, MD (T.A., G.F.T.); Dana-Farber Cancer Institute and Harvard Medical School (P.B.); Cardiac Arrhythmia Service, Massachusetts General Hospital, Boston, MA (P.T.E.); and West Virginia University, Morgantown, WV (M.R.M.).

The online-only Data Supplement is available with this article at http://circ.ahajournals.org/lookup/suppl/doi:10.1161/CIRCULATIONAHA.112.115592/-/DC1.

Correspondence to Anthony Rosenzweig, MD, Cardiovascular Division, Beth Israel Deaconess Medical Center, Center for Life Sciences, 3 Blackfan Cir, Boston, MA 02215. E-mail arosenzw@bidmc.harvard.edu

Circulation **is available at http://circ.ahajournals.org** **DOI: 10.1161/CIRCULATIONAHA.112.115592**

and in human heart disease, as well. To examine the functional role of chronic SGK1 activation, we generated cardiac-specific gain- and loss-of-function models through expression of constitutively active (CA) and dominant negative (DN) SGK1 mutants.[8] SGK1 activation comparable to that seen in failing hearts is sufficient to induce hallmarks of mechanical and electric remodeling. Interestingly, aspects of adverse remodeling could be reversed by ranolazine, suggesting a key role for the sodium current in the phenotype of the SGK1-CA transgenic mice. Conversely, genetic SGK1 inhibition mitigated the development of heart failure and fibrosis after TAC, and abrogated heart failure–associated biochemical changes in the sodium channel. Together these data suggest an important role for SGK1 in both the adverse electrical and mechanical remodeling seen in heart failure.

Methods

Generation of SGK1-CA and SGK1-KD Mice

All studies were approved by Institutional Animal Care and Use Committee. HA-tagged CA (S422D) and KD (K127M) mutants of SGK1 were subcloned downstream of the α-myosin heavy chain promoter in pbS2SK$^+$ (a generous gift from Dr Jeff Robbins, Cincinatti Children's Hospital). Linearized plasmids were microinjected into C57/BL6 oocytes and transferred to pseudopregnant mice as previously described.[12] Three independent lines were identified for each construct.

Transverse Aortic Constriction

Twelve-week-old male mice were subjected to TAC, as previously described with the use of a 25 gauge needle.[13] Perioperative mortality was not different between the wild-type and any of the transgenic lines studied.

Ischemia/Reperfusion Experiments

Twelve-week-old mice were subjected to 30 minutes of left anterior descending artery ligation and 24 hours of reperfusion as previously described.[12] The animals were monitored with continuous telemetry (Scisense data recording) during the time of ischemia and the first 45 minutes of reperfusion or until the animals had recovered from anesthesia.

Ranolazine Pellet Implantation

Two ranolazine pellets (14-day release, 140 mg/pellet, Innovative Research of America) were implanted subcutaneously in the intrascapular region. This dosage and formulation allows for stable plasma therapeutic levels of ranolazine (3–4 μmol/L) from 4 days onward after implantation.

Cardiac Function

Echocardiograms were performed on unanesthetized mice by the use of a GE Vivid5 with a 15L8 linear array transducer (13.0 MHz, imaging depth 10 mm) at a frame rate of 166 per second.

Hemodynamic studies were conducted on anesthetized mice (ketamine 100 mg/kg; xylazine 5 mg/kg) by using a 1.5F SciScience PV loop catheter (see online-only Data Supplement Methods).

In Vivo Electrophysiology Studies

Scisense octapolar electrophysiology catheters were advanced via the internal jugular vein to the right heart of mice anesthetized as above. With the use of an OctalBioamp stimulator (Medtronic) and AD data acquisition system, electrophysiology studies were conducted as described.[14] In brief, unipolar and bipolar electrograms were obtained from the right atrium, right ventricle, and left ventricle (LV), amplified, and filtered (event video recorder). Provocative testing was performed with double and triple extrastimulation, and rapid pacing, as well.

Tissue Harvesting

Mice were anesthetized and exsanguinated while the heart was perfusion fixed in situ with 4% paraformaldehyde at 100 cm H_2O (20 minutes) or removed and cryopreserved in liquid nitrogen for RNA and protein analysis.

Human Studies

Discarded pathological tissues were obtained and studied under an institutional review board–approved protocol.

Protein and RNA Analysis

Cardiac protein lysates were prepared, electrophoresed, and transferred to membranes for immunoblotting as described[15] and used with the following antibodies: total SGK1, p(thr256)SGK1, GSK3β, p(ser9)GSK3β, p(ser318)Foxo3A, p(ser253)Foxo3A (all from Cell Signaling); Ryanodine receptor, Nav1.5, Cav1.2a (all from Alomone); NCX (Gene Tex); SERCA (gift from Dr del Monte); SP-19, monoclonal antibody against SCN5a (Sigma); Nedd4-2, phospholamban, p(S16)Phospholamban, caveolin-3, GAPDH, HA tag (ABCAM). Immunoblots were scanned and bands quantified by densitometry. Only samples run on the same gel were compared for quantification.

Immunoprecipitation

Ventricular proteins were prepared in Cell Signaling lysis buffer (1% Triton) supplemented with protease (Thermo Scientific) and phosphatase inhibitors (Roche). Five hundred milligrams of protein was precleared with Protein A/G slurry (Calbiochem), immunoprecipitated with SP-19 (2 mg) or control IgG (3 hours, 4°C). Protein A/G slurry (40 mL) was then added to each tube and nutated for 90 minutes at 4°C. After several washes with phosphate-buffered saline buffer/0.1% Triton X-100 followed by phosphate-buffered saline /protease inhibitors (Thermo Scientific), protein was eluted with Laemmli sample buffer (37°C, 30 minutes), separated by using 4% to 20% gradient sodium dodecyl sulfate-polyacrylamide gel electrophoresis (BioRad), and immunoblotted as above.

SGK1 Kinase Assay

Ventricular proteins (500 mg) were immunoprecipitated with 2 mg of anti-SGK1 antibody (Upstate) with the use of Upstate Catch-and-Release columns. Immunoprecipitates were eluted by using nondenaturing buffer and incubated with 1 mg of SGK1 substrate (GSK3α/β fusion protein, Cell Signaling) and 200 mmol/L ATP (30 minutes, 30°C). Reaction products were separated by sodium dodecyl sulfate-polyacrylamide gel electrophoresis and detected by immunoblotting by using an antibody against phospho-ser 9/21 GSK3α/β (Cell Signaling).

Sucrose Gradient Analysis

Ventricular lysates were subjected to discontinuous sucrose gradient, and heavy membrane pellets, and supernatant fractions, as well, were collected and subjected to immunoblotting by using a modified version of a published protocol[16] (details in online-only Data Supplement Methods).

Histochemistry

Midventricular short axis sections were fixed (4% paraformaldehyde) and 5-mm sections stained with Masson trichrome to visualize fibrosis, wheat germ agglutinin staining to outline cardiomyocytes, and hematoxylin-eosin for cytoarchitecture. A prespecified, genotype-blinded image-selection method with the use of National Institutes of Health SCION software was used to quantify fibrosis (see online-only Data Supplement Methods).

Whole-Cell Patch Clamp Recording

Isolated ventricular myocytes were current and voltage clamped by using the whole-cell patch-clamp configuration as previously described.[17,18] Voltage and current clamp control and data acquisition

are performed with the use of custom-written software (see online-only Data Supplement Methods).

Biotin Surface Labeling

Neonatal rat ventricular myocytes were prepared as previously described[5] and plated at 1×10^6 cells/60-mm dish. Cells were grown in serum-containing media (Dulbecco's Modified Eagle's Medium, 10% horse serum, 5% fetal bovine serum, 1% glutamate) for 24 hours, then switched to serum-free media and infected with the indicated adenoviral vectors (multiplicity of infection, 50). After 48 hours, Pierce Cell Surface Protein Isolation Kit (Thermo Scientific) was used. In brief, cells were washed and labeled with Sulfo-NHS-SS-Biotin (30 minutes, 4°C). Cells were then washed and lysed, and biotin-labeled proteins were collected on a Neutravidin-agarose column. After elution, biotin-labeled proteins were subjected to sodium dodecyl sulfate-polyacrylamide gel electrophoresis and immunoblotting as above.

Statistics

Unless otherwise specified, data are expressed as mean±SEM. Distributions for continuous variables within each group were tested for normality by using the D'Agostino and Pearson omnibus normality test or Shapiro-Wilkes normality test if sample size was too small for the D'Agostino and Pearson text. Equality of variance between groups was tested by using the Bartlett test for equal variance. Mean comparisons between 2 groups were compared with the Student *t* test (normal distribution) or Mann-Whitney (nonnormal distribution) (Prism 5.0d for MAC). For multiple comparisons, 1-way analysis of variance (ANOVA) was performed, followed by the appropriate post hoc test as specified in the figure legends (Stata/IC 11.2 for windows or Prism 5.0d for MAC). For those subgroups with too few numbers to assess normality statistically, we validated parametric tests with appropriate nonparametric tests (Kruskal-Wallis test with post hoc Dunnett multiple comparison test or Mann-Whitney test for comparing 2 groups). For comparisons with 2 crossed factors, we performed 2-way ANOVA with post hoc Bonferroni test for multiple comparisons. In the experiments in which the 2-way ANOVA test could not be performed because of low sample size, we performed multiple *t* tests with adjustment for multiple comparisons by using a Bonferroni correction. For myocyte experiments, analysis was performed with repeated-measures ANOVA with random effect. Mortality data were quantified by using a *Z* test of proportions. For experiments with ranolazine in vivo, 2-factor repeated-measures ANOVA was performed; in addition, we also performed paired *t* tests between the pre and post groups for ranolazine and placebo groups.

Results

Cardiac SGK1 Is Activated in Heart Failure and Diet-Induced Insulin Resistance

We previously found that both activated or phosphorylated (thr-256)-SGK1 (pSGK1) and total SGK1 increase early after TAC-induced pressure overload (TAC).[5] SGK1 activity also remained elevated in chronic models of heart failure following TAC (TAC-HF) (Figure 1A). In contrast, neither phospho- nor total SGK1 were altered in a model of exercise-induced physiological hypertrophy (online-only Data Supplement Figure I).

To see whether SGK1 is altered in human heart disease, we examined ventricular tissue from patients with hypertensive heart disease (HHD, n=7) who died of noncardiac causes, and explants from patients with heart failure and dilated cardiomyopathy (n=10) at the time of orthotopic transplantation, as well. Healthy unused donor hearts served as controls (n=7). The cohorts were age and sex matched. Coronary angiograms had confirmed the lack of significant epicardial coronary artery disease in the patients with dilated cardiomyopathy, and gravimetry confirmed a trend toward increased LV mass in patients with HHD (control 363±133 g, HHD 518±112 g, $P=0.07$). In HHD hearts, there was an increase in total SGK1 (1.22±0.12, $P<0.05$) without a change in pSGK1 in comparison with controls (Figure 1B and 1C). Dilated cardiomyopathy hearts had a 2.3-fold increase in pSGK1 (2.3±0.85-fold, $P<0.005$ versus controls) without alterations in total SGK1 (Figure 1B and 1C).

These data suggest that SGK1 is abnormally regulated on multiple levels in human heart disease and murine models of hemodynamic stress but not in physiological hypertrophy.

Cardiac-Specific SGK1 Transgenic Mice

To investigate the functional role of SGK1 in the heart, we generated transgenic (TG) mice with cardiac-specific expression of either a CA (S433D) or a DN (K127M) SGK1 mutant[8] driven by the α-myosin heavy chain promoter.[19] Two of 3 independent SGK1-CA lines had increased early mortality and could not be maintained. A third line manifested normal viability and stable Mendelian inheritance and was investigated further. Two independent SGK1-DN lines had similar transgene expression and baseline phenotypes, and thus only one of these lines was characterized in detail. Immunoblotting for an incorporated hemagglutinin epitope tag confirmed cardiac-specific expression of both transgenes (online-only Data Supplement Figure IIA). SGK1 kinase activity was increased in SGK1-CA hearts at baseline to a level comparable to that seen in hearts from mice with TAC- HF (2.3-fold for TAC-HF, 2.9-fold for SGK1-CA TG mice versus wild-type (WT) mice, $P<0.05$ for both; Figure 1A). SGK1 activity in SGK1-DN hearts was no different from the low level seen in WT at baseline, but the increase in SGK1 kinase activity seen in TAC-HF WT mice was completely blocked in SGK1-DN mice (Figure 1A). These activity measurements were further supported by the observation that SGK1-CA increased phosphorylation of an SGK1-specific substrate (Foxo3A Ser-315/318[20]), whereas SGK1-DN blocked phosphorylation of this site after TAC (online-only Data Supplement Figure IIB and IIC). Phosphorylation of the Foxo3A-Ser-253 site, which is favored by Akt, was not altered (online-only Data Supplement Figure IIB). Thus, the SGK1-CA mice provide constitutive activation of SGK1 in a pathophysiologically relevant range at baseline, whereas the SGK1-DN mice act as an effective DN blocking the increase in SGK1 activity otherwise seen after TAC.

Gross and microscopic cardiac structure appeared normal in young adult (3–6 months old) SGK1-CA and SGK1-DN mice, including normal heart weight/body weight (HW/BW), head width/total length, and cardiomyocyte size. There was also no increase in fibrosis by Mason-Trichrome staining at these ages (online-only Data Supplement Table I and online-only Data Supplement Figure III). Echocardiography revealed normal left ventricular wall and diastolic chamber dimensions in both SGK1-CA and SGK1-DN TG at these ages. However, fractional shortening was reduced in SGK1-CA mice in comparison with the age-matched WT littermates (WT, 64±5%; SGK1-CA, 56±8%; $P\leq0.001$). SGK1-DN animals had normal function by echocardiography

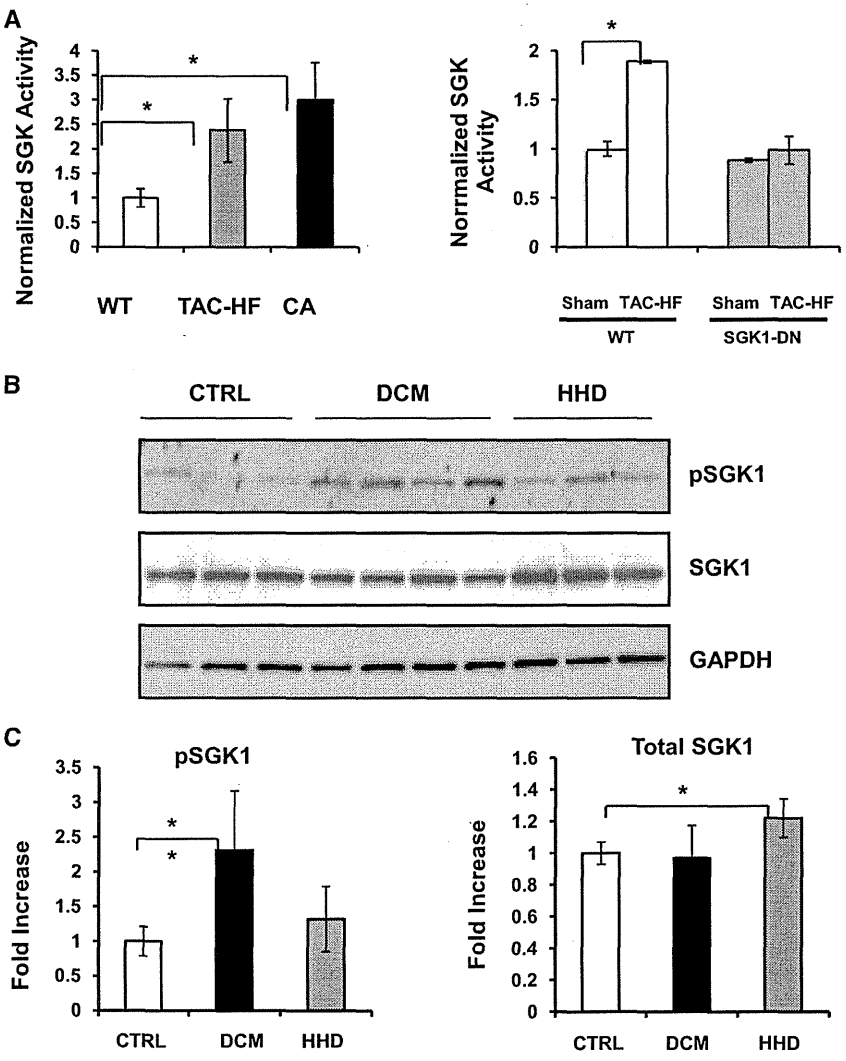

Figure 1. SGK1 activity is increased in murine and human heart disease. **A**, SGK1 kinase assays were performed on SGK1 immunoprecipitated from heart lysates. Data shown are mean±SEM normalized to WT sham-treated values in each group from 3 independent experiments (*P<0.05, the Welch t test with Bonferroni adjustment). **B**, Immunoblots of ventricular lysates from humans with healthy hearts who died of other causes (CTRL), patients with dilated cardiomyopathy (DCM) at the time of transplant, or patients with hypertension and increased LV mass (HHD), using an antibody against total- or phospho-SGK1. **C**, Cumulative quantitated data (mean±D for n=6–10 samples/group) normalized to GAPDH are represented as fold-change over control (*P<0.05, **P<0.001; 1-way ANOVA; Fischer-Hayter post hoc test). WT indicates wild type; SGK1, serum- and glucocorticoid-regulated kinase-1; LV, left ventricle; HHD, hypertensive heart disease; TAC, transverse aortic constriction; TAC-HF, TAC-induced heart failure; and ANOVA, analysis of variance.

(online-only Data Supplement Table I). To exclude potential confounding effects of fibrosis and sex, we focused subsequent experiments on 3- to 6-month-old male animals of each genotype.

Invasive hemodynamic studies confirmed that measures of systolic (dP/dt_{max} and preload recruitable stroke work) and diastolic (dP/dt_{min}, τ_g) function were depressed in SGK1-CA but not SGK1-DN mice (online-only Data Supplement Table II). Thus, at baseline, young adult SGK1-CA mice have mild but significant systolic and diastolic dysfunction without overt hypertrophy or fibrosis, whereas the SGK1-DN mice have normal cardiac structure and function.

SGK1 Activation Modulates the Response to TAC

To assess the role of SGK1 activation in the development of heart failure, we subjected SGK1-CA and SGK1-DN mice to TAC. Animals were euthanized either 4 (for SGK1-CA and WT littermates) or 7 weeks (for SGK1-DN and WT littermates) after TAC. The time points were dictated by our Institutional Animal Care and Use Committee policies that require animals be euthanized when they develop severe heart failure. At 4 weeks, TAC induced an increase in HW/BW and wall thickness in both SGK1-CA mice and WT littermates (online-only Data Supplement Figure IVA and IVB). However, SGK1-CA hearts were dilated with thinner walls and markedly reduced function (online-only Data Supplement Figure IVC and IVD). There was a nonsignificant trend toward increased fibrosis in the SGK1-CA in comparison with WT littermates after TAC (online-only Data Supplement Figure IVE). These data suggest that the baseline cardiac dysfunction seen with chronic SGK1 activation is markedly exacerbated by the additional stress imposed by TAC and accelerates progression to heart failure.

Both WT and SGK1-DN mice tolerated TAC better than SGK1-CA mice, and thus could be monitored longer after the intervention. Seven weeks after TAC, HW/BW ratios and LV wall thickness increased in both SGK1-DN and WT littermates in comparison with sham-operated controls (Figure 2A and 2B), although the change in HW/BW was less marked in SGK1-DN mice (Figure 2A). Echocardiography 7 weeks after TAC revealed reduced fractional shortening and increased LV dilatation (LV diastolic dimension) in WT but not in SGK1-DN mice (Figure 2C and 2D), probably accounting for the differences noted in HW/BW. SGK1-DN mice

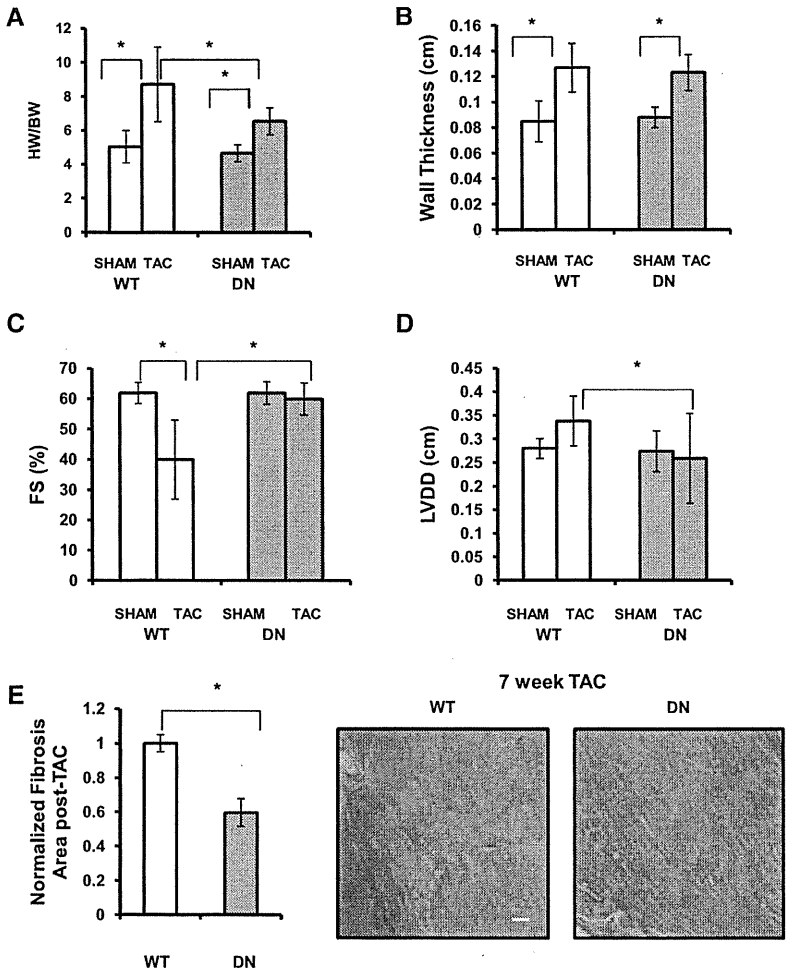

Figure 2. SGK1-DN mice are protected from heart failure after aortic constriction. **A** through **E**, Gravimetric, echocardiographic, and histological data from SGK1-DN and WT littermates 7 weeks after TAC or sham operation. **A**, HW/BW ratios showed significantly more LV mass in WT mice in comparison with SGK1-DN mice after TAC. **B** through **D**, Wall thickness, FS, and LVDD as measured by echocardiography 7 weeks after TAC showed that SGK1-DN mice are protected from LV dilatation and cardiac dysfunction in comparison with WT mice. **E**, Fibrosis is reduced in SGK1-DN in comparison with WT mice after TAC (inset shows representative Masson-Trichrome stain). *$P<0.05$ (2-way ANOVA with post hoc Bonferroni) n=10 in TAC groups, n=5 in sham groups. WT indicates wild type; SGK1, serum- and glucocorticoid-regulated kinase-1; TAC, transverse aortic constriction; FS, fractional shortening; DN, dominant negative; LV, left ventricle; HW/BW, heart weight/body weight; ANOVA, analysis of variance; and LVDD, left ventricular diastolic dimension.

also had less fibrosis than WT mice after TAC (Figure 2E). Thus, SGK1 inhibition protects against the development of heart failure, cardiac dilation, and fibrosis after pressure overload.

Altered Cardiac and Cellular Electrophysiology in SGK1-CA Mice

Because 2 of the 3 SGK1-CA TG lines had increased mortality and SGK1 is known to interact with ion channels, we investigated the electrophysiological effects of chronic SGK1 activation. ECGs in SGK1-CA mice revealed increases in R-wave amplitude, QRS duration, and QTc interval (QTc; 137±32 in SGK1-CA versus 100±12 ms in WT; $P<0.05$) without a change in RR or PR intervals (online-only Data Supplement Figure VA). In addition, spontaneous ventricular tachycardia was noted in a 12-month-old SGK1-CA mouse. SGK1-DN ECGs were not different from WT littermates (online-only Data Supplement Figure VB) and did not manifest ventricular arrhythmias. Holter monitoring for 2 weeks showed a trend toward increased premature ventricular activity, but, because of the sporadic nature of sudden cardiac death, we were not able to correlate mortality with ventricular arrhythmias in the SGK1-CA mice at baseline (online-only Data Supplement Figure VI).

To provoke ventricular arrhythmia, we performed intracardiac electrophysiological studies with the use of rapid ventricular pacing and programmed ventricular extrastimuli[14] in SGK1-CA, SGK1-DN, and WT littermates. Three of the 6 SGK1-CA mice studied had inducible polymorphic ventricular tachycardia with pacing to 90-ms cycle lengths. In contrast, more aggressive protocols with pacing to 60-ms cycle lengths did not induce ventricular tachycardia in any of the 9 WT and SGK1-DN mice studied ($P<0.05$ by Z test for proportions) (Figure 3A and 3B).

The induction of polymorphic ventricular tachycardia with pacing rather than programmed extrastimuli in the absence of significant fibrosis and structural heart disease was suggestive of triggered electric activity. Hence, we next examined the electrophysiological characteristics of cardiomyocytes isolated from SGK1-CA mice. Whole cell patch clamp of cardiomyocytes isolated from 3- to 5-month-old SGK1-CA mice demonstrated action potential prolongation over a range of pacing frequencies (0.5–4 Hz) in comparison with cardiomyocytes from WT littermates (Figure 3C). Early and delayed after-depolarizations, a hallmark of triggered electric activity, were also more frequent in SGK1-CA than in WT cardiomyocytes (Figure 3D). Thus, the increased ventricular arrhythmia seen in the SGK1-CA mice likely reflects an increase in triggered activity secondary to action potential prolongation.

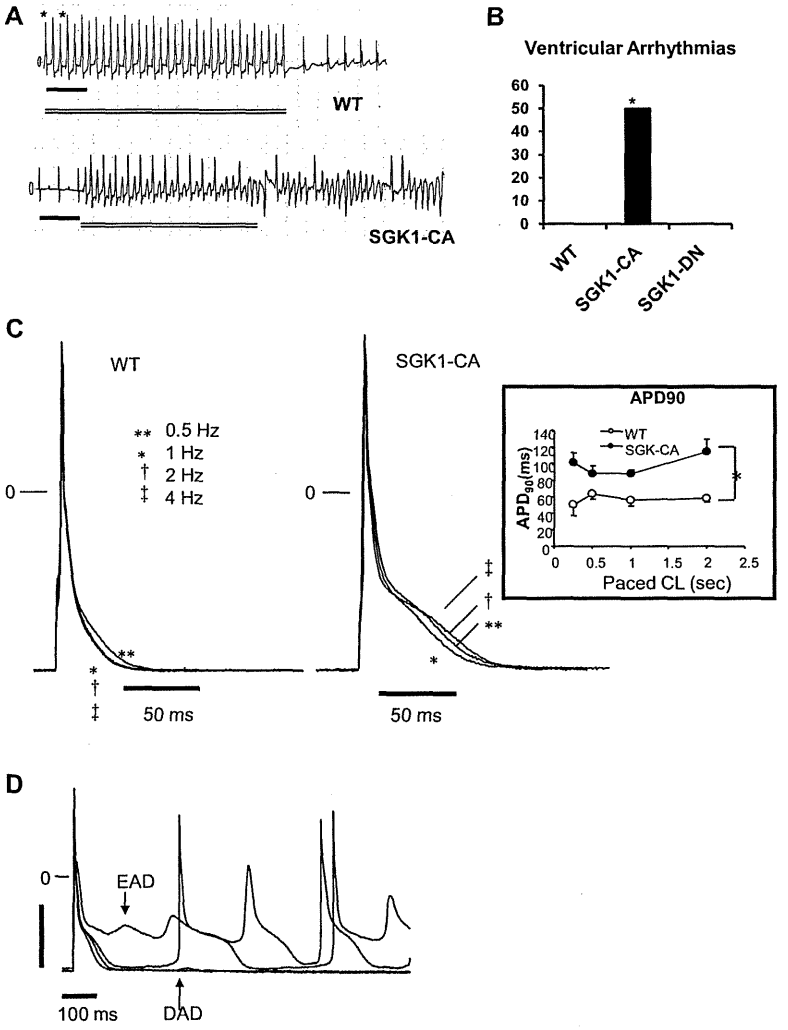

Figure 3. Propensity to ventricular arrhythmias, action potential prolongation, and after-depolarizations are increased in SGK1-CA mice. **A**, Representative tracings for WT and SGK1-CA mice from the distal (right ventricle) pole during rapid-pacing protocol (with pacing cycle lengths [CL] down to 60 ms in WT mice and 90 ms in the SGK1-CA mice). Asterisks denote pacing, double line indicates duration of pacing, and scale bar denotes 200 ms. **B**, Cumulative results for VT/VF inducibility from age-matched WT (0/5), SGK1-CA (3/6), and SGK1-DN (0/4) mice are shown (*$P<0.05$ by Z test of proportions), in the absence of fibrosis or structural abnormalities (online-only Data Supplement Figure III). **C**, Superimposed action potentials (APs) at CL 0.5 to 4 Hz in WT and SGK1-CA ventricular cardiomyocytes. **Inset**, APD at 90% repolarization (APD_{90}) was longer in SGK1-CA than in WT ventricular cardiomyopathies. *$P<0.05$ by repeated measures ANOVA. **D**, Representative EADs or DADs in SGK1-CA myocytes paced at 0.5 Hz. For quantification of EADs/DADs in comparison with WT see Figure 5D. WT indicates wild type; SGK1, serum- and glucocorticoid-regulated kinase-1; DN, dominant negative; CA, constitutively active; VT, ventricular tachycardia; VF, ventricular fibrillation; EAD, early after-depolarization; DAD, delayed after-depolarizations; and ANOVA, analysis of variance.

Regulation of I_{Na} by SGK1

An increase in APD could be secondary to altered potassium, calcium, or sodium currents. Whole cell patch-clamp analyses of cardiomyocytes isolated from SGK1-CA TG mice or WT littermates showed no differences in the peak potassium or calcium current densities (I_{to}, I_{K1}, or $I_{Ca,}$; online-only Data Supplement Figure VII). We also observed no difference in major calcium-handling proteins in cardiac sarcoplasmic reticulum or membrane preparations in SGK1-CA mice, with the exception of an increase in the sodium-calcium exchanger (NCX1) (online-only Data Supplement Figure VII). Overall, these data suggest that altered potassium or calcium currents are unlikely to account for APD prolongation and arrhythmias in SGK1-CA mice.

In contrast, whole cell patch clamp studies revealed substantial changes in sodium currents in SGK1-CA cardiomyocytes. Peak I_{Na} current density manifested a -10 mV hyperpolarizing shift (Figure 4A and 4B), in addition to increased peak current density in comparison with WT cardiomyocytes (Figure 4C). No difference was found in the reversal potential of I_{Na} between the SGK1-CA and WT mice cardiomyocytes.

To assess the effect of SGK1 activation on channel gating, we measured voltage-dependent activation and steady-state inactivation of I_{Na}. Cardiomyocytes from SGK1-CA mice showed a hyperpolarizing shift of -10 mV in the voltage dependence of Na^+ activation as illustrated in the conductance (G_{Na}) curves ($V_{1/2}$: -68.1 ± 4.0 versus -58.8 ± 4.4 mV, $P<0.001$), without altering the slope factor k (Figure 4D and online-only Data Supplement Table III). There was also a smaller negative voltage shift of -5 mV shift in I_{Na} steady-state inactivation in the SGK1-CA in comparison with WT cardiomyocytes ($V_{1/2}$; -83.9 ± 3.6 versus -77.8 ± 4.3 mV, $P<0.05$) (Figure 4D and online-only Data Supplement Table III). The combination of a large hyperpolarizing shift in the conductance–voltage relationship with a smaller hyperpolarizing shift of the steady-state inactivation leads to an increase in the window current, which would increase Na^+ conductance over a wider range of membrane potentials.[21,22]

SGK1 activation did not affect recovery from or entry into fast or intermediate inactivation (I_{IM}) (online-only Data Supplement Figure VIIIA and VIIIB and online-only Data Supplement Table III). Similarly, neither the fast nor slow time constants of I_{Na} decay were altered by chronic SGK1 activation (online-only Data Supplement Figure VIIIC and online-only Data Supplement Table III).

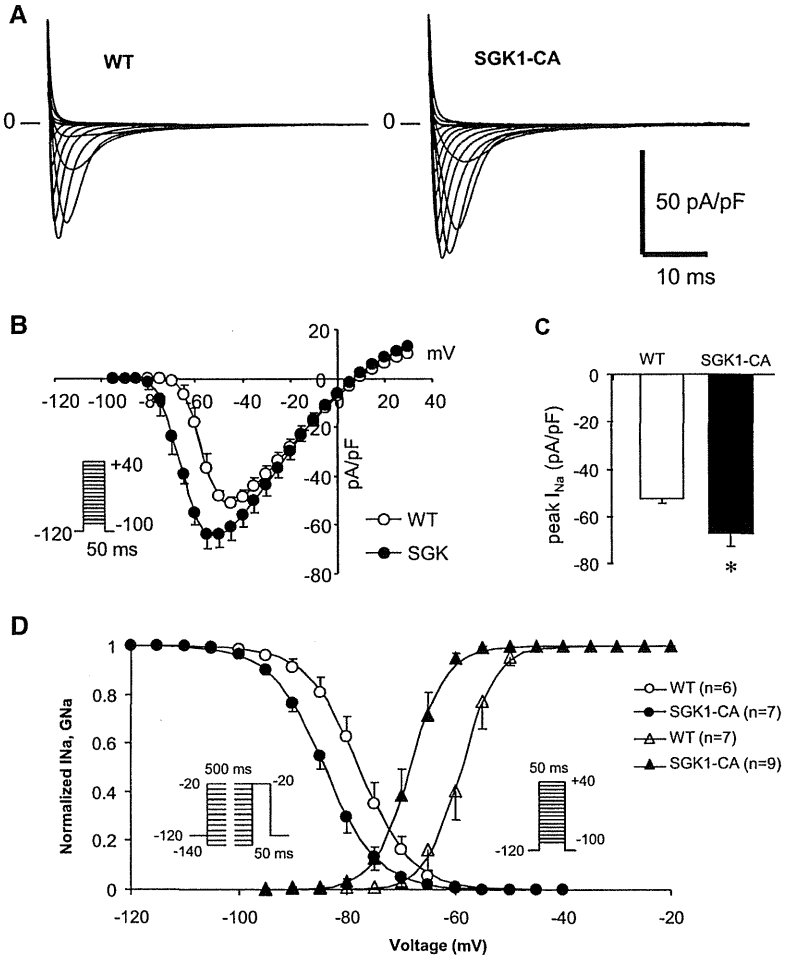

Figure 4. Sodium current density, activation and inactivation are altered in SGK1-CA cardiomyocytes. **A**, Representative I_{Na} currents in WT and SGK1-CA cardiomyocytes (10 mmol/L $[Na^+]_o$). **B**, Current–voltage (I-V) relationship for WT (n=7) and SGK1-CA (n=10) cardiomyocytes. **C**, Cumulative quantitation reveals peak I_{Na} density is increased in SGK1-CA (n=10) in comparison with WT (n=7) cardiomyocytes (*P<0.05, t test). **D**, Superimposed normalized conductance–voltage (G_{Na}–V) and steady-state inactivation curves from WT (○, n=6 and △, n=7, respectively) and SGK1-CA (●, n=7 and ▲, n=9, respectively) cardiomyocytes. There is a significant hyperpolarizing shift noted both in the voltage dependence of activation and steady-state inactivation of I_{Na} in SGK1-CA in comparison with WT. WT indicates wild type; SGK1, serum- and glucocorticoid-regulated kinase-1; and CA, constitutively active.

An increase in the persistent Na current, I_{NaL} and increases in window currents have been described in genetic arrhythmia and cardiomyopathy syndromes caused by mutations in the Nav1.5 sodium channel encoded by SCN5a,[23,24] and in acquired heart failure, as well.[25] SGK1-CA cardiomyocytes displayed a 3.6-fold increase in I_{NaL} in comparison with WT (0.87±0.29% versus 0.24±0.13%, P<0.01; Figure 5A). This increase is comparable to that seen with arrhythmogenic SCN5a mutations or acquired heart failure.[25]

Alteration of I_{Na} Plays a Key Role in the Phenotype of SGK1-CA TG Mice

To test the functional importance of increased I_{NaL} in SGK1-CA cardiomyocytes, we used ranolazine at low concentrations to selectively block I_{NaL}, without affecting peak I_{Na}.[26] Ranolazine treatment normalized APD in SGK1-CA cardiomyocytes without affecting APD in WT cardiomyocytes (Figure 5B and 5C). Moreover, ranolazine treatment reduced the number of SGK1-CA cardiomyocytes with after-depolarizations (early and delayed after-polarizations) to the background level seen in WT cardiomyocytes (Figure 5D). These data strongly suggest that SGK1 activation leads to APD prolongation and increased after-depolarizations primarily through increasing I_{NaL}.

To investigate the role of increased I_{NaL} in this model in vivo, we examined the effects of ranolazine on SGK1-CA TG mice at baseline and in a model of ischemia–reperfusion, in which I_{NaL} has been implicated in ventricular arrhythmias.[27,28] SGK1-CA TG mice had substantially higher mortality (80%) than either WT (24%, P=0.002) or SGK1-DN mice (12.5%, P=0.0006) (Figure 6A). Because the majority of SGK1-CA mice were dying in the first hour after reperfusion, we subjected the mice to continuous telemetry during the 30 minutes of ischemia and the first 45 minutes of reperfusion or until the mice had recovered from anesthesia. Interestingly, SGK1-CA mice had a higher incidence of lethal ventricular arrhythmias during ischemia–reperfusion than WT mice (4 of 5 in SGK1-CA versus 0 of 4 in WT, P=0.02) (Figure 6A and 6B).

To investigate the role of I_{NaL} in vivo, we implanted ranolazine slow-release pellets subcutaneously in SGK1-CA mice in comparison with placebo pellets (Figure 6C). Seven days after implantation, both the QT and QT_c intervals were decreased in ranolazine-treated in comparison with placebo-treated animals (Figure 6D). Remarkably, echocardiography also revealed that fractional shortening was better in ranolazine-treated in comparison with placebo-treated mice (Figure 6E). Evaluation of change from baseline fractional shortening by paired t tests demonstrated a nonsignificant trend toward improvement in ranolazine-treated mice (P=0.055) but no difference in placebo-treated animals

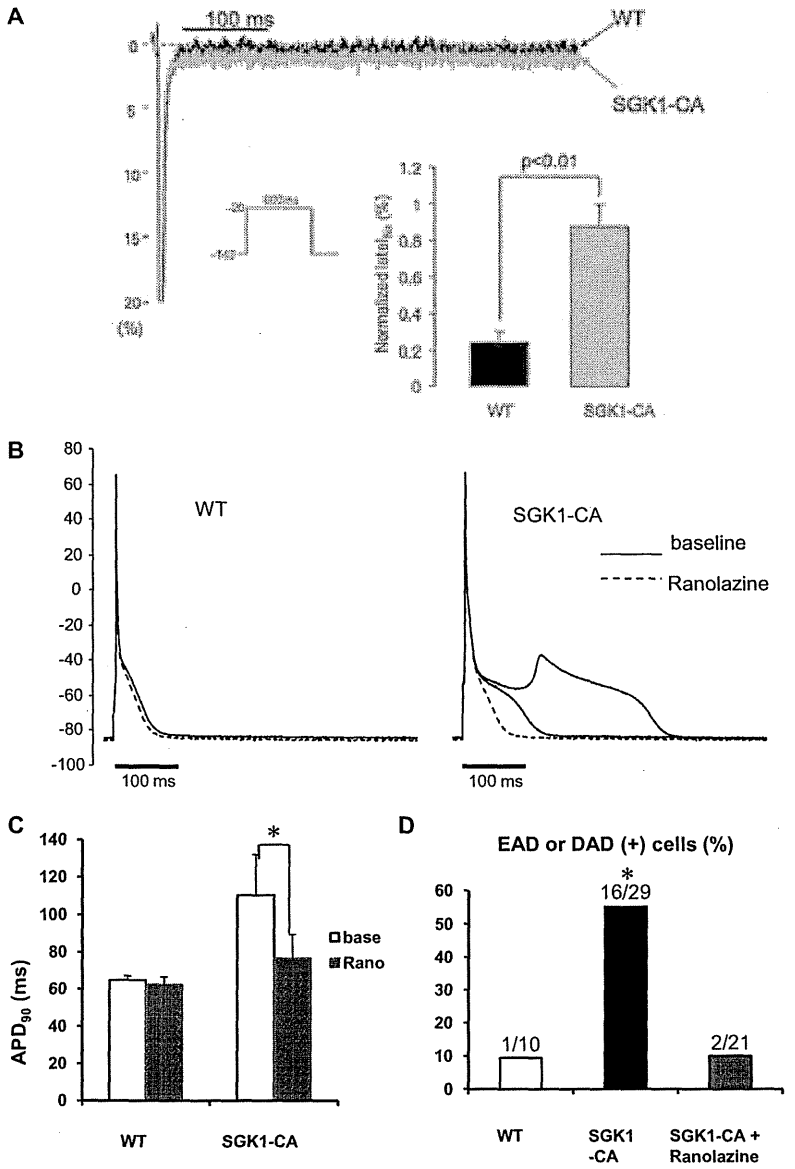

Figure 5. SGK1 activation increases I_{NaL}, whereas ranolazine normalizes APD and suppresses after-depolarizations in SGK1-CA cardiomyocytes. **A**, Representative normalized I_{NaL} (% of peak) superimposed for WT and SGK1-CA cardiomyocytes. **Inset** shows that normalized I_{NaL} was larger in SGK1-CA (n=6) than in WT cardiomyocytes (n=5). **B**, Superimposed APs in cardiomyocytes from WT and SGK1-CA mice before (baseline: solid line) and after ranolazine (dotted line) at 0.5-Hz pacing. Ranolazine (1 μmol/L) normalized APD and suppressed EAD in SGK but did not affect APs in WT myocytes. **C**, Ranolazine (1 μmol/L) normalized APD_{90} in SGK1-CA cardiomyocytes (*P<0.05, repeated-measures ANOVA), but did not affect APD_{90} in WT cardiomyocytes. **D**, EADs and DADs were more frequent in SGK1-CA than in WT cardiomyocytes. Ranolazine (1 μmol/L) reduced after-depolarizations in SGK1-CA cardiomyocytes (*P<0.05 by χ^2 test) to levels seen in WT cardiomyocytes. WT indicates wild type; SGK1, serum- and glucocorticoid-regulated kinase-1; CA, constitutively active; EAD, early after-depolarization; DAD, delayed after-depolarizations; AP, action potential; APD, action potential duration; Rano, ranolazine; and ANOVA, analysis of variance.

(P=0.59). The small number of animals in this complex protocol obviously limits the statistical power for such inferences. Nevertheless, these findings are provocative and suggest that the role of SGK1-mediated changes in sodium currents in adverse mechanical remodeling should be addressed more fully in future studies. Finally, ranolazine treatment markedly reduced the incidence of lethal ventricular arrhythmia (1/5) in comparison with either untreated (4/5; Figure 6A) or placebo-treated SGK1-CA mice (3/3) (Figure 6F). Taken together, these data strongly support the hypothesis that increased I_{NaL} is responsible for the ventricular arrhythmia seen in SGK1-CA mice, paralleling our in vitro studies, and suggest that I_{NaL} may also contribute to the cardiac dysfunction seen with SGK1 activation in vivo.

SGK1 Is Necessary and Sufficient for Heart Failure–Associated Alterations in Nav1.5

To understand the biochemical basis for the functional changes seen in I_{Na}, we examined Nav1.5, the primary pore-forming subunit of the cardiac voltage-gated sodium channel complex. Although there was no change in overall cardiac Nav1.5 protein expression in SGK1-CA or SGK1-DN mice in comparison with WT, sucrose gradient fractionation[29] demonstrated that the subcellular distribution of Nav1.5 was altered by both TAC-HF and SGK1 activation in a similar way. In sham-operated WT mice, a large proportion of Nav1.5 was localized to lipid rafts with a modest amount of Nav1.5 in the heavy membrane (HM) fraction, likely comprising both intercalated disc and sarcoplasmic reticulum proteins (online-only Data Supplement Figure IXA, top). TAC-HF and SGK1-CA hearts had similar increases in Nav1.5 in the HM fraction (online-only Data Supplement Figure IXA, middle and bottom). In contrast, although the baseline Nav1.5 distribution in SGK1-DN hearts was similar to that in sham-operated WT, the increase in HM Nav1.5 seen in WT mice following TAC was markedly decreased in SGK1-DN hearts (online-only Data Supplement Figure IXB).